

Tidal Resource Characterization from Acoustic Doppler Current Profilers

Jeffrey Epler

A thesis  
submitted in partial fulfillment of the  
requirements for the degree of

Master of Science in Mechanical Engineering

University of Washington

2010

Program Authorized to Offer Degree: Department of Mechanical Engineering

University of Washington

Graduate School

This is to certify that I have examined this copy of a master's thesis by

Jeffrey Epler

and have found that it is complete and satisfactory in all respects,  
and that any and all revisions required by the final  
examining committee have been made.

Committee Members: Brian Polagye, Jim Thomson, Phil Malte

---

Brian Polagye

---

Jim Thomson

---

Phil Malte

Date:

---

University of Washington

Abstract

Tidal Resource Characterization from Acoustic Doppler Current Profilers

Jeffrey Epler

Chair of the Supervisory Committee:

Doctor Brian Polayge

Department of Mechanical Engineering

A compelling aspect of power generation from tidal currents is the predictability of the resource, which is generated by the gravitational pull of the Sun and Moon on the Earth's oceans. This thesis focuses on the characterization of tidal currents, using data obtained from both stationary and shipboard current meters.

For technical feasibility studies, it is presupposed that once the currents at a site have been well characterized it is possible to make accurate predictions of the electricity that would be generated by an array of turbines. These data are generally collected by Acoustic Doppler Current Profilers (ADCP), which use active acoustics to measure currents throughout the water column. For this purpose, ADCPs are commonly deployed on the seabed and configured to measure and record the currents over relatively long periods of time (i.e., greater than 28 days). From these time series data, harmonic analysis is used to describe the observed tidal currents as a series of superimposed periodic components (each describing forcing from the relative orientation and position of the Earth, Sun, and Moon), and these components provide a basis for future predictions. From stationary ADCP deployments collected over the last year in Admiralty Inlet, WA, harmonic analysis of the velocity time series has produced harmonic fits which account for at least 94 % of the variation in the velocity data. By combining two ADCP deployments, amplitude ratios and phase corrections of the P1 and K2 tidal constituents were determined for inference with shorter time series. The harmonic analysis

removes over 99 % of the variance in the diurnal and semi-diurnal frequency bands and has provided spatial mapping of current strength variability in the survey area.

Where tidal currents vary significantly over a small area such as Admiralty Inlet, WA, shipboard ADCP surveys can be utilized to provide an efficient method to characterize the variability. Balancing spatial coverage (track length) and resolution (ship speed) is important to achieve meaningful accuracy in the results. For example, in areas with large gradients in tidal phase, a single survey over a large area cannot distinguish differences in the fundamental strength of the currents at a location and from the stage of the tide at which those currents were measured. An approach developed for this location involves multiple laps during a tidal cycle around a short “racetrack”, with the shipboard ADCP continuously measuring velocity profiles. An acceptable spatial resolution is achieved by a 20 minute racetrack lap with speed over ground no faster than 5 knots. Faster vessel speeds tend to result in poor ADCP signal returns. Each racetrack lap is divided horizontally into 100 x 100 m bins and vertically into 5 m bins, creating an ensemble volume for individual measurements collected on each lap. The velocity time series for each volumetric ensemble is then approximated as sine curve using unconstrained non-linear optimization to find amplitude, phase, and period of the curve. The key assumption in this analysis is that each tidal cycle can be adequately represented by a sine wave, which is supported by the periodic nature of tidal currents. Surveys during ebb currents demonstrate consistent normalized current amplitude variation giving resolution of differences over scales  $O(100\text{ m})$ . Differences in phase of the peak ebb currents throughout the site are less conclusive due to the low temporal sampling of the racetracks. However, flood surveys show variation in timing of up to an hour with minor variation in peak strength. The relative amplitude trends are consistent between cycles of differing strength and time of the year, as confirmed by multiple surveys over a nine month period.

# TABLE OF CONTENTS

	Page
LIST OF FIGURES.....	ii
LIST OF TABLES .....	iv
1 Introduction.....	1
1.1 Tidal Current Devices.....	1
1.2 Tides & Currents .....	4
1.3 Site Description & Tidal Current Resource .....	8
1.4 Data Collection.....	10
1.5 Acoustic Doppler Current Profilers - Principles of Operation .....	12
1.6 Admiralty Inlet Characterization - Tidal Energy Metrics .....	15
2 Stationary Analysis.....	18
2.1 Literature Review .....	18
2.2 Methodology .....	26
2.3 Results & Discussion.....	30
3 Mobile Analysis .....	43
3.1 Literature Review .....	43
3.2 Methodology .....	47
3.3 Results & Discussion.....	56
4 Conclusion .....	62
References .....	63
Appendix 1- Rayleigh Criterion Constituent Inclusion Charts.....	66
Appendix 2 - Shallow Water Constituent Inclusion Criteria .....	67

## LIST OF FIGURES

Figure Number	Page
Figure 1 – OpenHydro Tidal Turbine.....	3
Figure 2 – Marine Current Turbine (MCT), SeaGen Tidal Turbine .....	3
Figure 3 – The tractive forces between the Earth and Moon.....	4
Figure 4 – Diagram of the Spring & Neap Cycle of the Earth-Moon-Sun System.....	5
Figure 5 – Spring & Neap, Perigean & Apogean, Tropic & Equatorial Cycles of Currents .....	6
Figure 6 – Average Daily Maximum Tide Range.....	7
Figure 7 – Map of Puget Sound and Admiralty Inlet .....	8
Figure 8 – Bathymetric map of Admiralty Inlet with SnoPUD survey area.....	9
Figure 9 - OpenHydro Tidal Turbine .....	10
Figure 10 – Stationary data collection package (sea spider).....	11
Figure 11 – Stationary Sea Spider Deployments .....	12
Figure 12 – Teledyne RDI Workhorse Sentinel.....	13
Figure 13 – ADCP, upward looking.....	14
Figure 14 – Single Ping Data Distribution & Ensemble Averaged Data Distribution .....	15
Figure 15 – Distances between selected sea spider deployments .....	17
Figure 16 – Tidal Ellipse .....	23
Figure 17 – NOAA Tidal Current Predictions vs. ADCP.....	25
Figure 18 – Histogram of differences between NOAA slack water timing.....	25
Figure 19 – Comparison of raw ADCP data vs. post averaged data .....	28
Figure 20 – Path traced out by tip of current vector over one tidal cycle.....	29
Figure 21- Principal axis rotation.....	30
Figure 22 – Amplitude inference results .....	32
Figure 23 – Phase inference results.....	33
Figure 24 – ADCP signed speed, T Tide harmonic fit, residual .....	34
Figure 25 – Power spectral density .....	37
Figure 26 – Raw Signed Speed Signal, Hamming filter (red), Tapered Signed Speed .....	38
Figure 27 – M2 constituent amplitude (m/s) from stationary ADCP deployments .....	39
Figure 28 – M2 constituent phase (deg) from stationary ADCP deployments .....	40
Figure 29 – Shipboard ADCP ebb survey track in Admiralty Inlet from August 2009. ....	49
Figure 30 – Vessel path from all shipboard ADCP ebb and flood surveys .....	50
Figure 31 - Individual pings with bin centerlines and outlines from August, 2009 .....	52
Figure 32 - Individual ADCP ping velocity profiles for August 2009 ebb survey .....	52
Figure 33 – Histogram of ADCP Pings w/ Normal PDF.....	53

Figure 34 - Ensemble averaged data with half period sine fit .....	54
Figure 35 – Normalized peak ebb current amplitude .....	57
Figure 36 – Peak ebb current phase .....	58
Figure 37 - Normalized peak flood current amplitude. ....	59
Figure 38 - Peak flood current phase.....	60
Figure 39 - Ensemble averaged data with quarter sine fits.....	61

## LIST OF TABLES

Table Number	Page
Table 1 – Traditional Hydrokinetic Site Metrics for Admiralty Inlet .....	16
Table 2 – Lunar Time and Astronomical Variables Developed.....	18
Table 3 – Tidal Constituents Ranked by Tidal Potential.....	19
Table 4 – Stationary Tripod Deployments: ADCP properties .....	26
Table 5 – Percent Variance Fit by Harmonic Analysis (hub height $\approx 10$ m).....	35
Table 6 – R-squared values for harmonic approximation (hub height $\approx 10$ m) .....	35
Table 7 – Signed Speed and Residual Variance in Diurnal and Semidiurnal bands .....	37
Table 8 – $t_{tide}$ amplitude and phase results with 95% confidence intervals .....	41
Table 9 – Shipboard ADCP Configuration.....	47
Table 10 – Shipboard ADCP survey summary from Admiralty Inlet.....	51

## ACKNOWLEDGMENTS

I would like to thank Doctor Brian Polagye for his teaching and mentoring me. Our discussions on my research and the development of new methods for using shipboard ADCP surveys was invaluable. His enthusiasm and motivation for the development of tidal energy inspired my own research as well as interest in the future of developing this energy resource. I would like to thank Doctor Jim Thomson for his willingness to explain instrumentation and discuss concepts used in my research and Doctor Phil Malte for his general support and interest in my progress since last autumn. At the University of Washington Applied Physics Lab, I want to thank both Joe Talbert for his expertise with assembly, deployment, recovery, and turnaround of the SeaSpider and essentially getting all of my data back to me, and Captain Andy Reay-Ellers for his diligence in completing repetitive ship tracks in Admiralty Inlet for hours at a time.

I would like to give a sincere thank you to Doctor Roy Martin for his generous fellowship support over the last nine months. Without his support none of my research would have been possible.

Lastly, a thanks to all my family and friends who have been supportive and shown interest in my education and research over the last two years.

## **1 Introduction**

The realization and development of clean and renewable energy is important to the future of power generation throughout the world, due the impacts from fossil fuel use, including global climate change. Existing and new demands for power generation must be met with renewable technology which can alleviate the strain on the environment and also impose minimally itself. Around the world there has been considerable development in wind energy over the last twenty years. Currently, wind energy projects are a feasible power generation option and an attractive asset in a power company's portfolio. At this time, tidal energy and wave energy find themselves in the same position that wind industry was in twenty years ago, with many concepts trying to move to market. Hydrokinetic tidal energy devices generate power by harnessing the kinetic energy in periodic tidal current motion. While it is possible to leverage some of the existing knowledge base from the wind energy industry, tidal hydrokinetic power generation faces unique challenges, which and has triggered research on the resource, environmental effects, and device design. Unlike wind or wave energy, tidal current energy involves extracting energy from a deterministic resource generated by the gravitational pull of the Sun and Moon on the Earth's oceans. Therefore, while the resource is intermittent, it is predictable.

Here in Washington State, there is a public drive to be a leader in renewable energy. For example, under Initiative 937, by 2020 a utility company must generate at least 15 % of its power from renewable sources excluding conventional hydroelectric. In Puget Sound, both Snohomish County Public Utility District (SnoPUD) and Navy Region Northwest are in the beginning stages of testing pilot scale tidal turbine projects. SnoPUD aims to deploy a pilot project in Admiralty Inlet and the Navy off of Marrowstone Island. The economic feasibility of a project depends directly on the strength of the currents and mean spring peak currents of 2-2.5 m/s is an approximate threshold for project feasibility as estimated by Fraenkel [12].

### **1.1 Tidal Current Devices**

Since power generation from tidal currents is in the very first stages of development, there are a wide variety of device concepts. The primary device classification is based upon rotor orientation. Device rotors are either horizontal axis (axis of rotation parallel to flow) or vertical axis or cross-flow (axis of rotation perpendicular to flow) devices. In most cases, the rotor converts the power in the currents

into rotational mechanical power using hydrodynamic lift. The lift creates mechanical rotation and is coupled through a drive train to an electric generator. Devices are designed to operate on both directions of the tide above a cut-in speed (typically around 1 m/s). Horizontal axis devices are most common, borrowing from the wind energy industry where horizontal axis wind turbines are used in large scale, commercial wind farms. Other concepts, including oscillating hydrofoils, vortex induced vibration, and hydrodynamic drag rotors, are at even earlier stages of commercialization.

One useful metric to assess the power generation potential of a site is the kinetic power density ( $P$ ) which depends on the cube of velocity;

$$P = \frac{1}{2} \rho v^3 \quad (\text{W/m}^2)$$

where  $\rho$  is the seawater density (nominally  $1024 \text{ kg/m}^3$ ) and  $v$  is the current velocity (m/s). For comparison a wind turbine rated at 2 MW, 12 m/s wind speed would have average power production of 700 kW from a device with 45 m blade radius. A tidal turbine with maximum current speeds of 3 m/s and 9 m blade radius would have comparable average power production. This disparity is due to the large difference between the density of air and water (a factor of 800).

Foundation structures or moorings are designed to withstand the maximum forces on the rotors. Foundations may be secured to the seabed using anchors (pilings) driven in to the sea floor or using gravity based foundations which resist rotor forces by friction against the seabed. For pile foundations, the overall footprint on the bottom of the device is smaller than for an equivalent device using a gravity foundation. However, the maximum feasible installation depth for pile foundations is around 50m [24].

In Figure 1 and Figure 2 are two horizontal axis tidal turbine devices which are currently in testing. The OpenHydro device was installed in 2009 in the Bay of Fundy by Nova Scotia Power and generates 200 kW with a current of 2.5 m/s and blade diameter of 10 m. At peak generation, the rotor turns at 12 rpm. The foundation is a gravity-based tripod and the rotor is fixed allowing no yaw (ability to change rotor direction) of the rotor [24].



**Figure 1 – OpenHydro Tidal Turbine. (Source: OpenHydro)**

The Marine Current Turbine seen below was installed off the coast of Ireland at Stranford Lough in 2008, and has a fixed piling foundation. This device is would generate 1600 kW in currents of 2.5 m/s from both 16m diameter blades. At peak power generation, the rotor turns at 14.3 rpm [24].

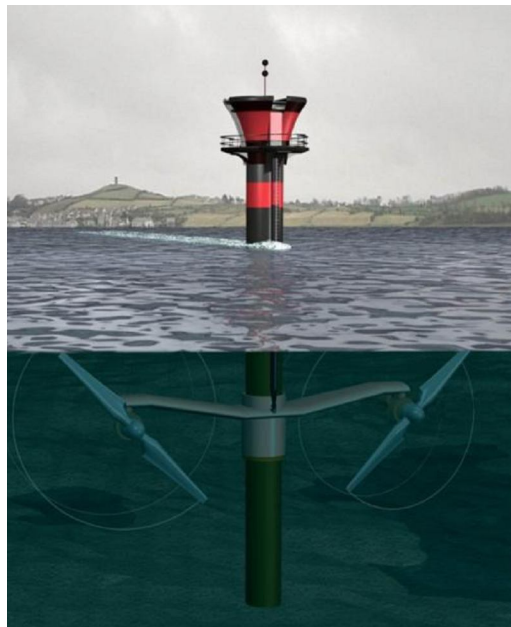


**Figure 2 – Marine Current Turbine (MCT), SeaGen Tidal Turbine. (Source: EERE 2010)**

These are just two of numerous devices which are in the development stages. Since tidal energy is such a new industry, no superior design has yet emerged, leaving plenty of opportunities for future innovation.

## 1.2 Tides & Currents

Gravitational forcing between the Earth, Sun, and Moon drives both tides and currents, processes which were first observed by Galileo and subsequently explained by Newton's Law of Universal Gravitation. As the Earth and Moon rotate around a common barycenter (center of mass of both bodies) the interaction of centrifugal and gravitational forces between the bodies is constantly changing, both temporally and spatially over the Earth. At different latitudes on the Earth's surface, the gravitational force between the Earth and the Moon changes direction while the centrifugal force direction stays the same. The misalignment between the gravitational and centrifugal forces result in a differential force (magnitude and direction). The differential force has both normal and parallel force components acting at the surface of the Earth. The parallel components are known as tractive forces and result in a pull on the oceans towards the Moon creating a tidal bulge or concentration of water mass towards the closest point from the Earth to the Moon. The bulge corresponds to a higher water level (high tide). In the idealized, equilibrium situation, as the tidal cycle progresses from low to high tide, the difference in volume means water must be coming into the area horizontally to change the volume vertically. These horizontal movements of water are the tidal currents. Just as the Moon creates a set of tractive forces a similar set of forces exist between the Earth and Sun.

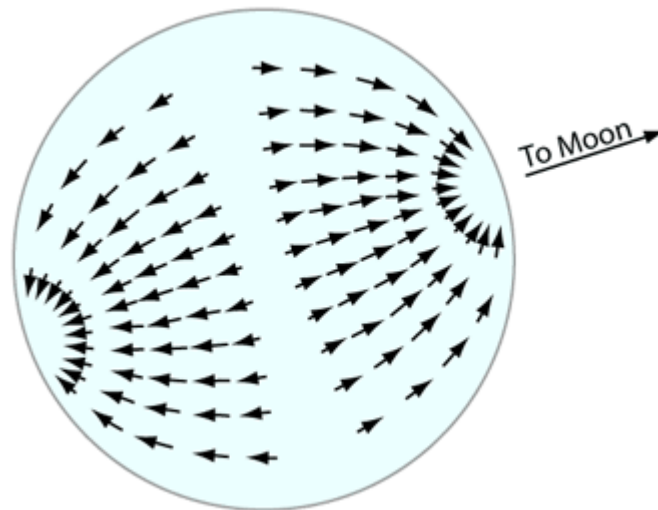


**Figure 3 – The tractive forces between the Earth and Moon. (Source: <http://www.oc.nps.edu> 2010)**

Because both the Moon and the Sun impose tractive forces upon the Earth, the total tractive force seen by the oceans is due to the superposition of the two. As seen above in Figure 3, the tractive

force for the Moon or Sun is directionally aligned to the axis between the Earth and celestial body. Due to this superposition, when the Earth, Moon, and Sun are aligned along the same axis, this results in a peak in tractive forces, known as a spring tide. When the alignment between the Earth and Moon and Earth and Sun are offset 90 degrees, the tractive forces of each body act to reduce the resultant tractive forces, leading to a minimum condition known as a neap tide. The spring/neap cycle has a period of 14.76 days and is seen below in Figure 4. Tides and currents are classified by their general periodic behavior. At the extremes are purely diurnal (1 cycle / day) and semi-diurnal (2 cycles / day) tides. However, mixed tides with both diurnal and semi-diurnal characteristics are most common.

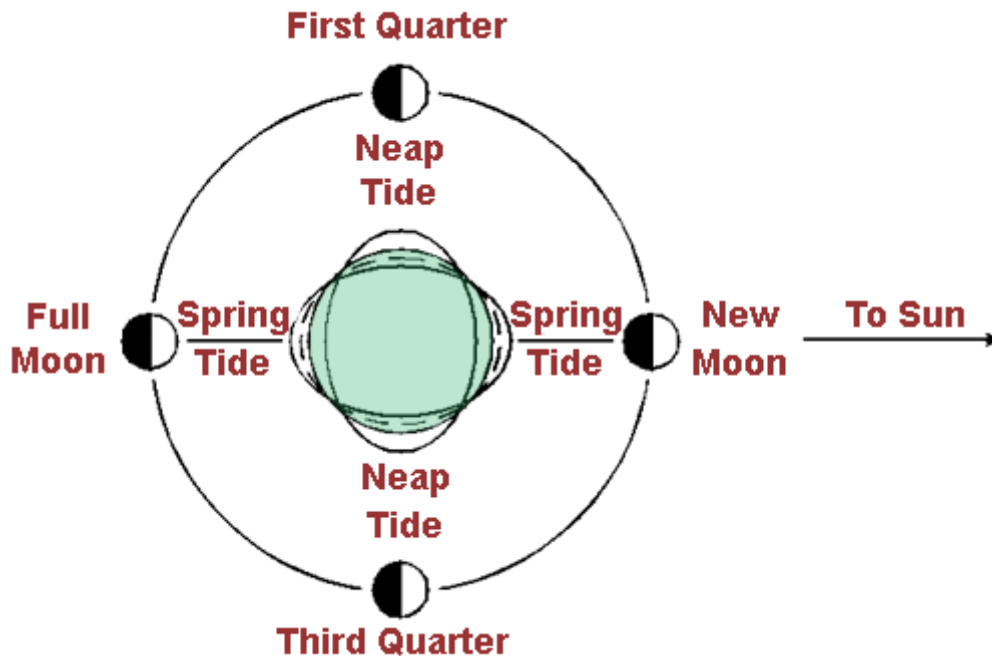


**Figure 4 – Diagram of the Spring & Neap Cycle of the Earth-Moon-Sun System. Source <http://www.oc.nps.edu/nom/day1/partc.html>, May 1, 2010.**

In addition to spring and neap variation in tides and currents, the orbit of the Moon around the Earth is elliptical and the minimum distance and maximum distances are called the lunar perigee and apogee, respectively. The elliptical variation of the Moon's orbit causes an intensification of tides and currents when the Moon is closest and is periodic with the lunar month (27.55 days – perigean and apogean tides). A third pronounced periodic behavior is the tropic and equatorial cycle (13.66 days), representing the maximum inclination of the Moon relative to the Earth's equator. This leads to a diurnal inequality, in which there are two tidal cycles per day, but one cycle is considerably weaker than the other (tropical tide). When the Moon is over the equator, the inequality reduces considerably (equatorial tide). Below in Figure 5 is a representation of currents over a month, which shows the previously explained cycles.

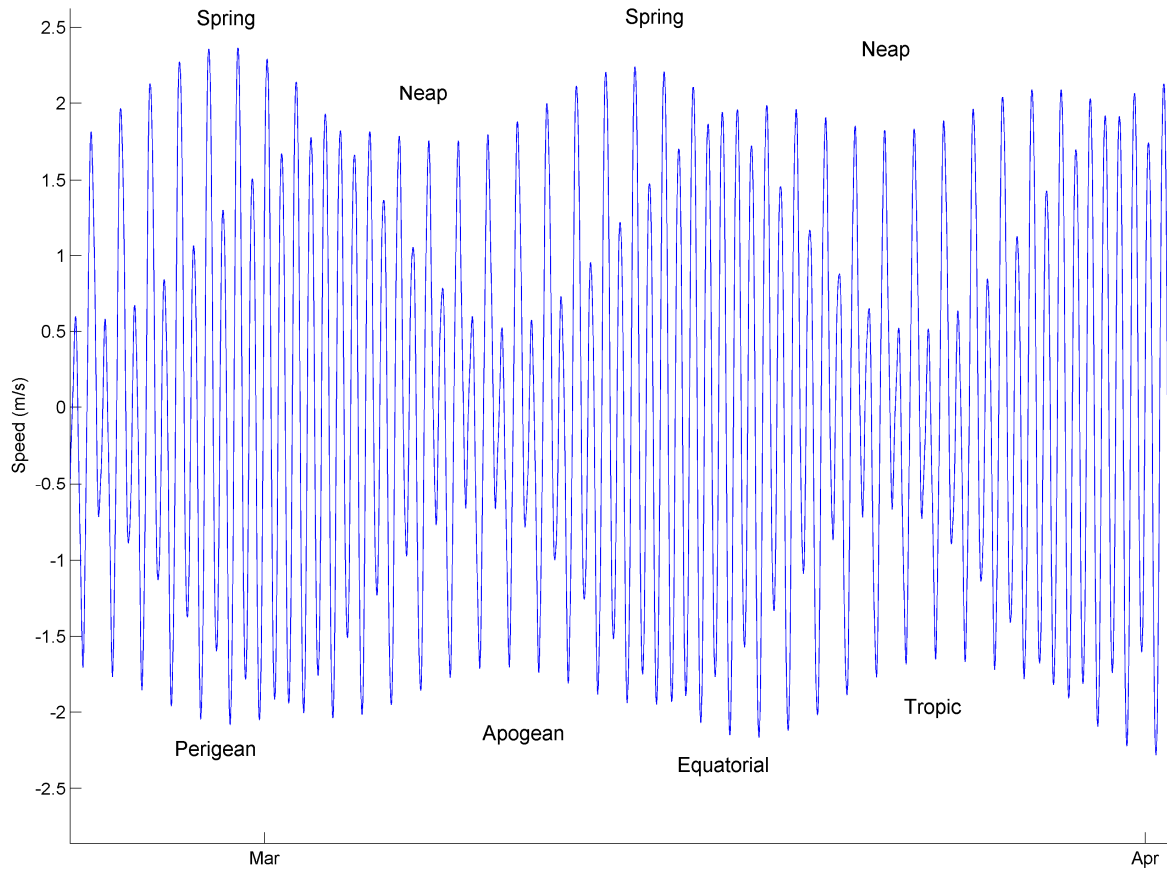


**Figure 5 – Spring & Neap, Perigean & Apogean, Tropic & Equatorial Cycles of Currents**

As the water levels oscillate between high tide and low tide, there are large changes in total water volume, this difference is the tidal prism. If the tidal cycle is moving towards high tide, water flows horizontally towards a coastline or basin, filling up the tidal prism. The horizontal flow of water that fills the prism are known as currents and driven by horizontal pressure gradients due to the rise and fall of the tides. Currents which move landward are flood currents and outgoing currents are ebb currents. Because of the continual rotation of the Earth, Moon, and Sun, the Earth's oceans are never in equilibrium with the tractive forces. The constant variation of the tractive force interacting with land masses, create a global inequality of tidal height and current strength. In Figure 6 the global variation of tidal range can be seen.

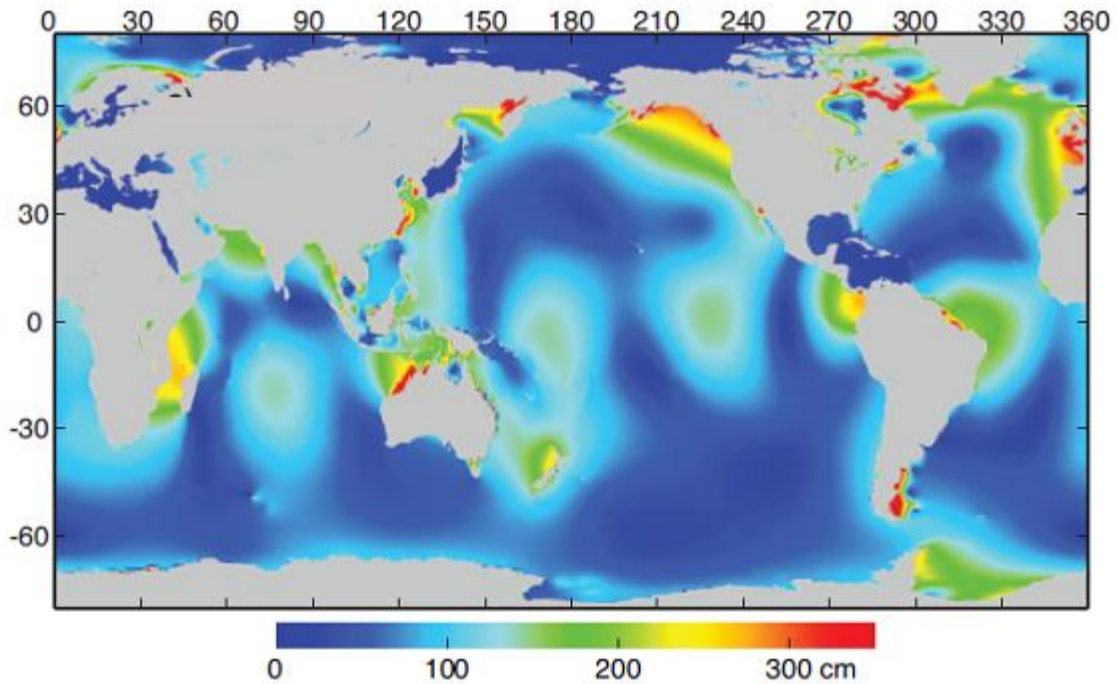


**Figure 6 – Average Daily Maximum Tide Range.** (Source: <http://www.pacificstormsclimatology.org/images/glossary/tides.png>)

Tidal range is minimal in the open ocean and maximum in bays and estuaries where the interaction of the forcing with basin topography can amplify the tides through resonance. Currents are driven by the same processes as tidal heights, yet have fundamental differences. Tidal heights are a one dimensional (scalar) process while tidal currents are three dimensional varying considerable with depth and horizontal position. Tidal currents have considerable variation over distances  $O(100\text{ m})$ , especially when bathymetry and topography changes are pronounced in an area. The interaction of strong currents with bathymetry and topography can lead to turbulence in the currents. Density stratification can lead to residual currents which are not controlled by gravitational forcing. Currents due to the gravitational forces on the body of water are classified as “tidal” while currents due to large scale ocean circulation and metrological conditions are “non-tidal”. In coastal waters, barotropic currents (forced by gravitational effects) are tidal and baroclinic currents (forced by density stratification) are non-tidal. Tidal currents are predictable because they are generated by a periodic astronomical forcing. Non-tidal currents are often stochastic and are more difficult to forecast.

### 1.3 Site Description & Tidal Current Resource

This thesis focuses on northern Admiralty Inlet, Puget Sound, Washington, but the methods presented should also be applicable to other potential tidal energy sites. Puget Sound is a fjord estuary approximately 240 km long and has a combination of deep basins and shallow sills. Admiralty Inlet, at the northern end of Puget Sound, is the major entrance and has strong currents due to the tidal exchange through the relative constriction of the channel cross-section. At the constriction between Point Wilson and Admiralty Head, Admiralty Inlet is roughly 5 km across and has a 60 m mean depth. This is considerably shallower than the Strait of Juan de Fuca and main Puget Sound basin which has depths up to 280m. The astronomical forcing of water over the Admiralty Inlet sill results in strong currents, exceeding 3 m/s during a strong spring tide. Seattle, well south of Admiralty Inlet has much weaker currents (mean maximum ebb and flood less than 0.2 m/s). Conversely, the mean tidal range of Seattle (2.32m) is considerably larger than that of Port Townsend (1.59m) [19]. Below is a map of the entire Puget Sound with an enlargement of Admiralty Inlet.

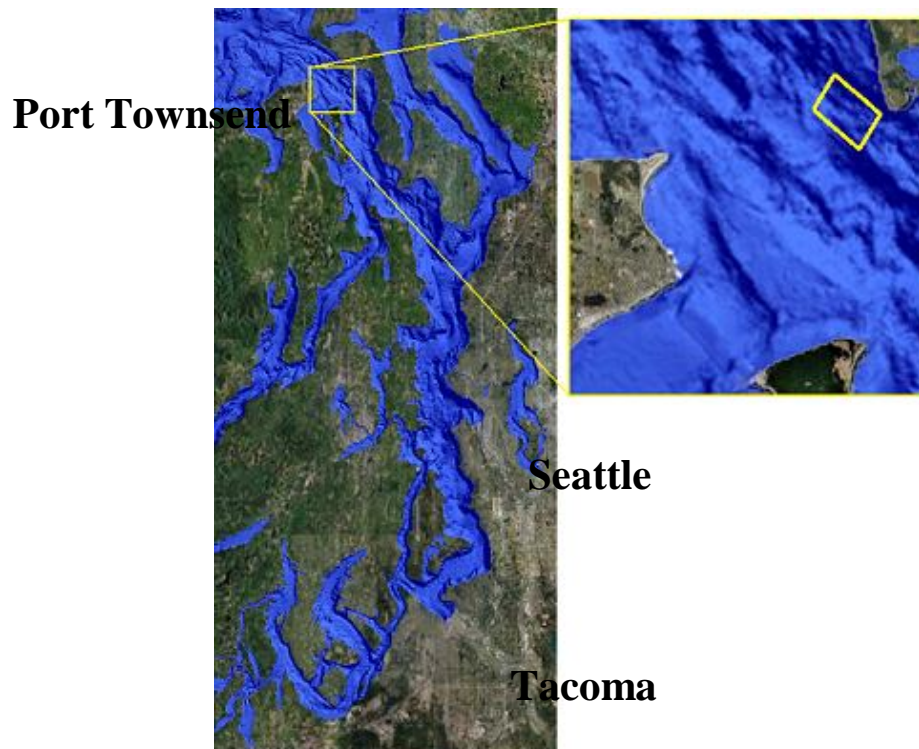


**Figure 7 – Map of Puget Sound (left) and Admiralty Inlet (right). Northern Admiralty Inlet survey area , 1 x 1.5 km (right, yellow). Bathymetric data from Finlayson [7].**

Because of the scouring effect of such strong currents, the seabed is composed of cobbles (10-20cm diameter) with very little sediment. Currents ebb (outflow) and flood (inflow) into Puget Sound twice a day of unequal strengths, making Puget Sound a mixed mainly semi-diurnal estuary. Seen below, the bathymetry of the site is extremely diverse, resulting in significant spatial variations in currents. Identifying spatial variations in current velocity is extremely important for device performance due to the sensitivity of the kinetic power density of a flow to small changes in velocity.

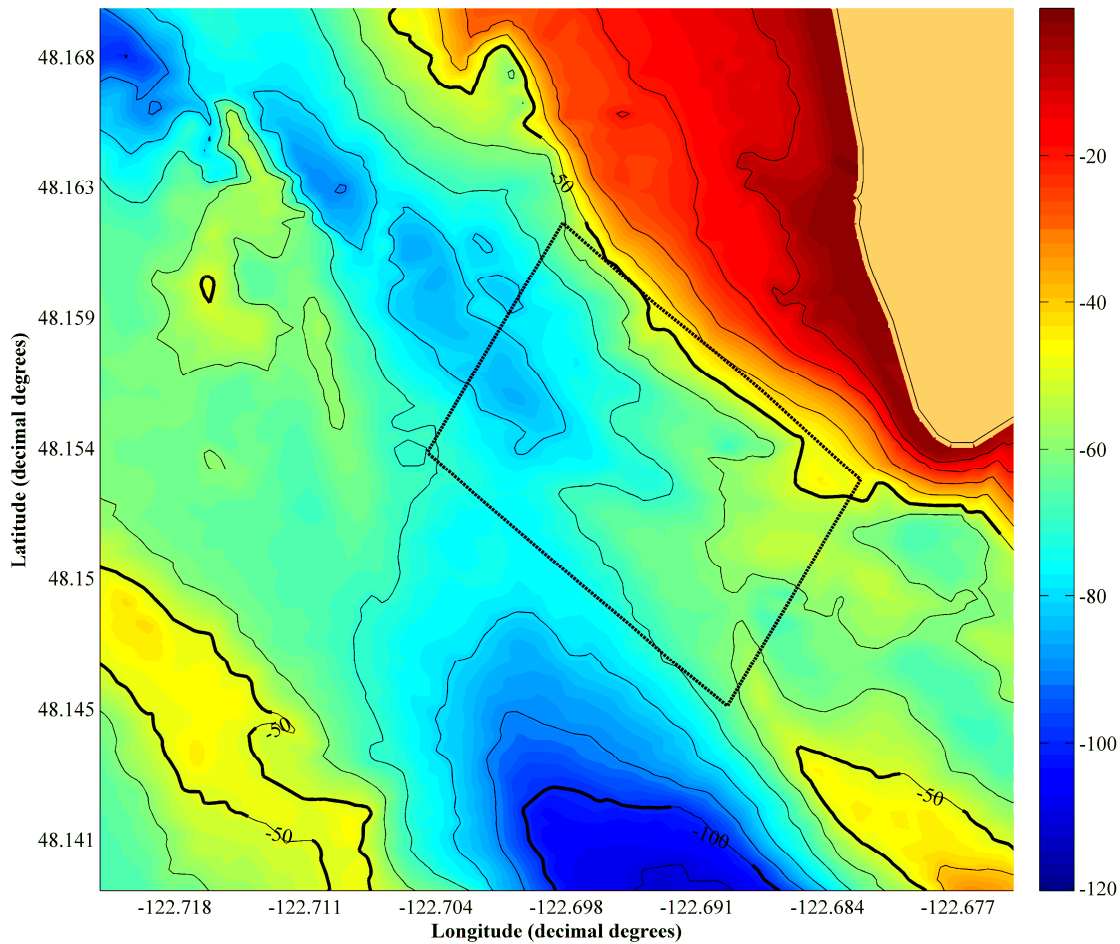


**Figure 8 – Bathymetric map of Admiralty Inlet (mean depth  $\approx$  60m) with SnoPUD survey area (dashed black line)**

Snohomish County Public Utility District (SnoPUD) is attempting to obtain permits for a pilot scale tidal energy project in Admiralty Inlet, off of Admiralty Head. The partnership between SnoPUD and University of Washington researchers has led to an extensive and ongoing research effort to characterize the physical and biological environment at this site. This site is under development because of a number of desirable characteristics:

1. Intense tidal resource with only moderate levels of turbulence;
2. Deep enough to avoid disruption of navigation of ship traffic, but not too deep for device installation;
3. Many existing users, but potentially enough space to minimize conflict with those users;
4. Relatively flat, rocky seabed; and
5. Potential for commercial build-out at conclusion of a successful pilot project.

SnoPUD intends to deploy two OpenHydro, horizontal axis tidal turbine devices in this location. Each turbine is 10 m in diameter, with a 10 m hub height, and generates peak power of 500 kW. The defining features of the OpenHydro design are a shroud enclosing the high solidity rotor, the open rotor center, direct-drive permanent magnet generator, and gravity foundation.

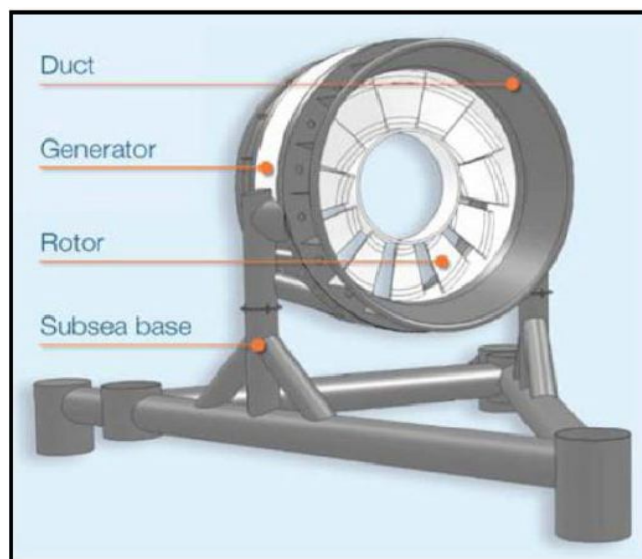


**Figure 9 - OpenHydro Tidal Turbine.** (Source: [http://www.snopud.com/Site/Content/Documents/tidal/ai/11-ExhibitF\\_LargeFormat.pdf](http://www.snopud.com/Site/Content/Documents/tidal/ai/11-ExhibitF_LargeFormat.pdf))

#### **1.4 Data Collection**

In order to characterize the SnoPUD survey area, a mix of oceanographic measurements is required. These may be conducted from a research vessel or from a stationary platform on the seabed. Mobile measurements from aboard a ship are used to characterize spatial variations at a similar moment in time, while stationary measurements are used to characterize temporal variations at a single location.

Stationary measurements collected by stand-alone instrumentation are also limited by the availability of on-board power and data storage.

The stationary, stand-alone instrumentation platform (Sea Spider, manufactured by Oceanscience, Oceanside, CA) deployed in Admiralty Inlet includes a suite of instruments to quantify the physical and biological dynamics of the site. Instruments measure velocity, background noise, water quality (temperature, salinity, dissolved oxygen), and echolocation activity by marine mammals. Figure 10 shows the components of the instrumentation package.

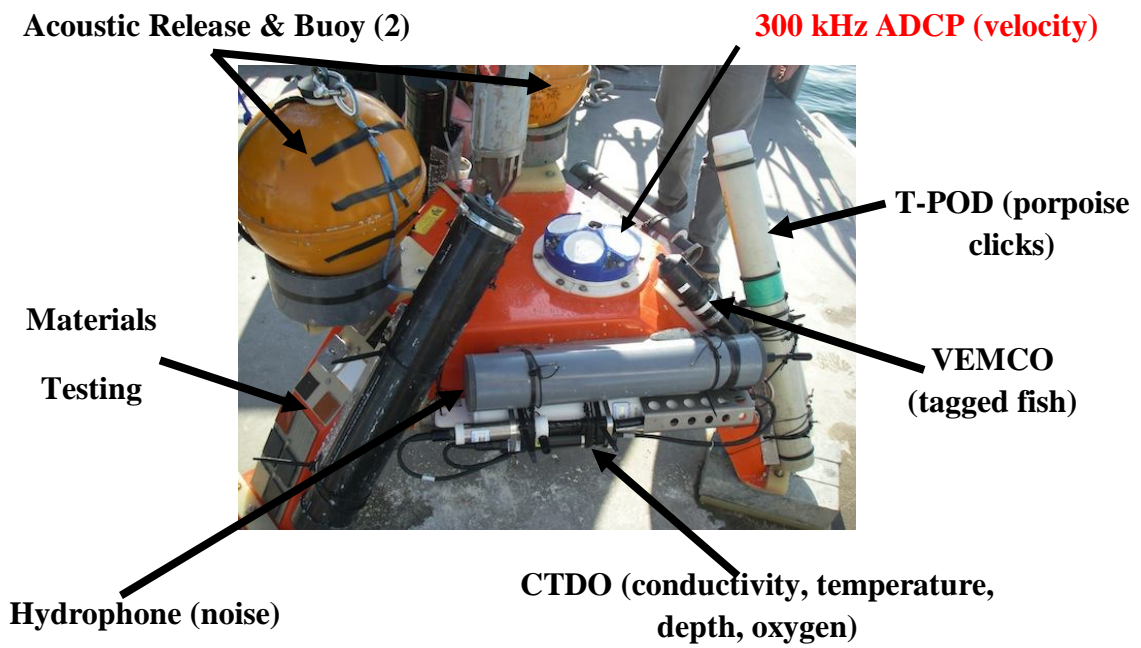


**Figure 10 – Stationary data collection package (sea spider)**

The platform is ballasted by over 600 lbs of lead, which is barely sufficient to hold the platform in place (on the first strong spring current after deployment, the ADCPs internal heading sensor has recorded changes in heading of over 90° as the feet of the tripod slide over the cobbled seabed). The locations of all instrumentation deployments to date are shown in Figure 11. The two deployments from 2007 which are outside of the survey region were conducted by Evans Hamilton, a Seattle-based oceanographic consultancy. The red triangle is the proposed deployment area for the SnoPUD pilot project and future work will focus on this location.

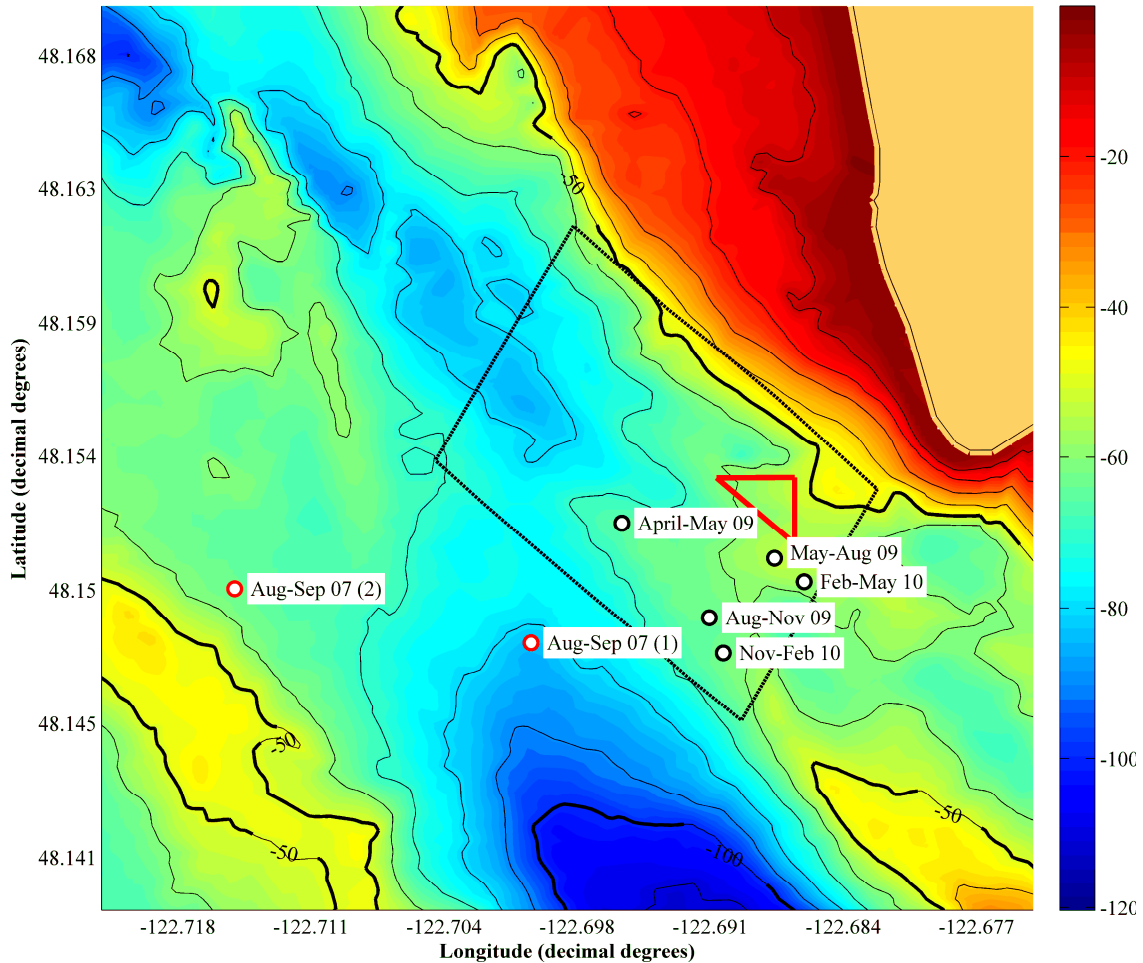


**Figure 11 – Stationary Sea Spider Deployments**

In addition to stand-alone instrumentation at the site, ship-based measurements of noise, velocity, and water quality been conducted during the retrieval and redeployment of the instrumentation platform (every three months). This thesis focuses on velocity data collected by an Acoustic Doppler Current Profiler during both stationary and shipboard surveys in order to characterize currents in Admiralty Inlet.

### **1.5 Acoustic Doppler Current Profilers - Principles of Operation**

Acoustic Doppler Current Profilers (ADCPs) are oceanographic instruments which measure the velocity of the water. This is accomplished by transmitting a sound pulse at a fixed frequency and listening for the Doppler shift in echoes returned from sound scatterers in the water column.

Scatterers include particulate and plankton and a key assumption in the measurement is that the scatterers themselves have very little mass and, therefore, act as a Lagrangian particles. The specific model of ADCP used to collect data in Admiralty Inlet (Teledyne RDI Workhorse Sentinel) is shown in Figure 12.



**Figure 12 – Teledyne RDI Workhorse Sentinel**

The Doppler shift is the difference between the frequency which is transmitted and the frequency which is reflected off of a moving particle back to the source. Broadband ADCPs produce a measurement of velocity with low uncertainty because of the large bandwidth with which velocity is sampled. They operate on the principle of time dilation rather than on direct measurements of phase. Time dilation is the difference in time taken for a sound pulse to travel to and back from a particle which is moving vs. a particle which is stationary. Doppler frequency shift and time dilation are conceptually equivalent. Issues do arise when trying to resolve the phase differences caused by time dilation of the returned pulses. Echoes never come from a single scatterer but from a cloud of scatters which distorts and complicates the echo. Echoes are compared to the transmitted pulse using autocorrelation, a comparison of the transmitted pulse with itself over differing time lags.

Each transducer on an ADCP sends and receives its own Doppler shifted pulse (ping) and can only measure the velocity normal to the transducer head. Therefore, in order to estimate the velocity in Earth coordinates, information from three beams at different orientations are required. Beams are all equally offset from vertical (defined as perpendicular of) and each beam measures the Doppler shift of particles at slightly different horizontal locations for each depth bin. However, beam spreading is sufficiently small that is generally acceptable to assume a horizontal homogeneity, especially in shallower waters. When four beams are used (as for the Teledyne RDI workhorse), an estimate of horizontal velocity and two, independent estimates of vertical velocity are made. The difference

between the two vertical velocity estimates is termed the “error velocity” and is indicative of horizontal heterogeneity. Along beam uncertainties are also factored into the error estimates.

ADCPs do not just measure the currents at a point but instead over an entire depth range building up a water velocity profile. This is done by using the speed of sound in water to estimate how long after the transmit pulse is sent that a response should be expected from a specified distance away. Knowing when to listen for the echo from different distances from the transducer is known as range gating. The profile is broken up into vertical bins (depth bins) in which the velocities are averaged using a weight function about the center of the bin. These profiles provide information about both horizontal and the vertical components throughout the water column.

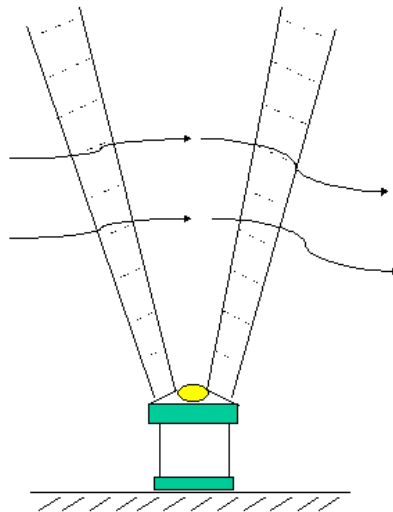


**Figure 13 – ADCP, upward looking, each dashed black line can be thought of as a depth bin. (Source: [web.vims.edu/physical/research/TCTutorial/currentmeasure\\_files/image002.gif](http://web.vims.edu/physical/research/TCTutorial/currentmeasure_files/image002.gif))**

Each ADCP “ping” obtains a velocity profile. However, a single ping has high uncertainty [6], which can be reduced by ensemble averaging (Figure 14). Ensemble averaging reduces random noise in the velocity measurements by minimizing the impact of a single highly noisy ping and can either be done internally by the ADCP or during post processing of the ADCP measurements. The standard deviation reduces with  $N^{-0.5}$  ( $N$  is ensemble size), making longer ensembles less noisy. However, because ensemble averaging assumes that the velocity field is stationary over the averaging period, long ensemble periods may smooth out real variations in the measured currents. The bias in the measurement cannot be reduced with ensemble averaging and can be thought of as constant, long-term measurement error.

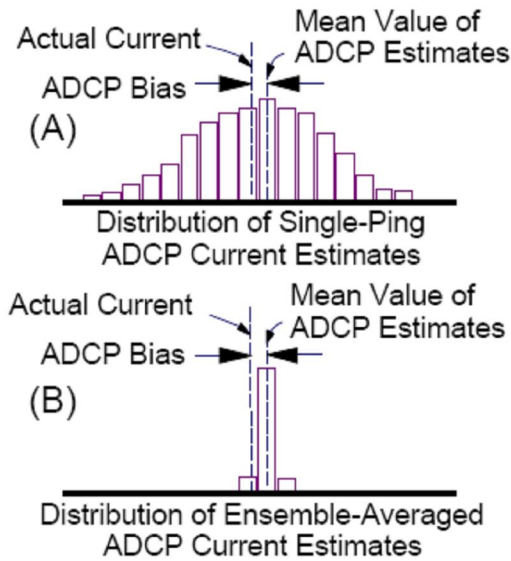


**Figure 14 – Single Ping Data Distribution (A), Ensemble Averaged (200 Pings) Data Distribution (B).**  
**Source: Gordon [17]**

When configuring an ADCP for a stationary deployment, there are trade offs between range, temporal resolution, and random noise. Range is the vertical resolution of the profile and the total profiling distance from the ADCP. As the vertical resolution increases (smaller bin size) the standard deviation of the ensembles also increases due to a decrease in transmitted pulse length. High temporal resolution increases the amount of data which needs to be stored and requires high sampling rates which can drain battery life faster than desired. Random noise is reduced through ensemble averaging (battery draining) or increasing bin size (loss of vertical resolution). Shipboard ADCP surveys have no power limitations allowing for maximum resolution, ping rate, and data storage of individual pings.

ADCPs are a crucial tool for mapping tidal currents for hydrokinetic device siting and play a key role in siting decisions for hydrokinetic tidal turbines.

## 1.6 Admiralty Inlet Characterization - Tidal Energy Metrics

A number of metrics may be derived from the stationary ADCP data to characterize the currents in Admiralty Inlet.

Table 1 presents a comparison of velocity, power, and directional metrics between the NNMREC sea spider deployments and the two deployments by Evans Hamilton in 2007. These metrics are described in Gooch [16].

**Table 1 – Traditional Hydrokinetic Site Metrics for Admiralty Inlet. Source: Brian Polayge, UW NNMREC**

Measurement	AH	PW	1	2	3	4	5
Date			4/09 – 5/09	5/09 – 8/09	8/09 – 11/09	11/09 – 2/10	2/10 – 5/10
<b>All Tides</b>							
<b>Velocity</b>							
Mean speed (m/s)	0.8	0.8	0.9	1.2	1.0	0.9	1.1
Max sustained speed (m/s)	2.4	2.5	2.4	3.2	2.4	2.7	3.0
Ebb/flood asymmetry	1.1	0.9	1.1	1.2	1.1	1.1	1.1
Vertical shear (m/s per m)	0.03	0.03	0.02	0.04	0.03	0.03	0.03
<b>Power</b>							
Mean power density (kW/m <sup>2</sup> )	0.6	0.7	0.9	1.7	0.8	0.8	1.4
Ebb/flood asymmetry	1.6	0.8	1.3	1.6	1.3	1.0	1.4
<b>Direction</b>							
Principle axis (deg)	136	132	141	127	133	127	108
Standard deviation (deg)	20	9	14	13	14	15	14
Ebb/flood asymmetry (deg)	13	5	18	20	26	28	31
<b>Site</b>							
Assumed hub height (m)	10	10	10	10	10	10	10
Mean depth (m)	78	69	65	54	58	62	48
Measurement duration (days)	32	32	40	75	97	78	82
Vertical resolution (m)	2	1	1	1	1	1	1
Sampling interval (min)	15	15	10	0.5	2.25	0.75	1.00

- *Mean Speed:* Average of all velocity magnitudes during ebb, flood, and slack water
- *Max Sustained Speed:* Highest velocity magnitude sustained for at least 5 minutes
- *Ebb/flood asymmetry:* Ratio of mean velocity magnitude during ebb to flood, ( $v_{\text{ebb}}/v_{\text{flood}}$ )
- *Vertical shear:* Ratio of change in velocity magnitude above and below hub height to depth
- *Mean Power Density:* Mean of kinetic power densities from each velocity measurement
- *Ebb/flood asymmetry:* Ratio of mean ebb power density to mean flood power density
- *Principal Axis:* Angle to true north of the ebb/flood cycle that captures the maximum variance in the data
- *Standard Deviation:* Deviation of ebb and flood about the principal axis

- *Ebb/flood asymmetry*: Difference principal axes of ebb and flood when found for each regime

Recalling the spatial locations of each deployment from Figure 11, the differences between sites can be quantified. To better understand the length scales over which there is considerable variation Figure 15 shows approximate distances between stationary deployments.

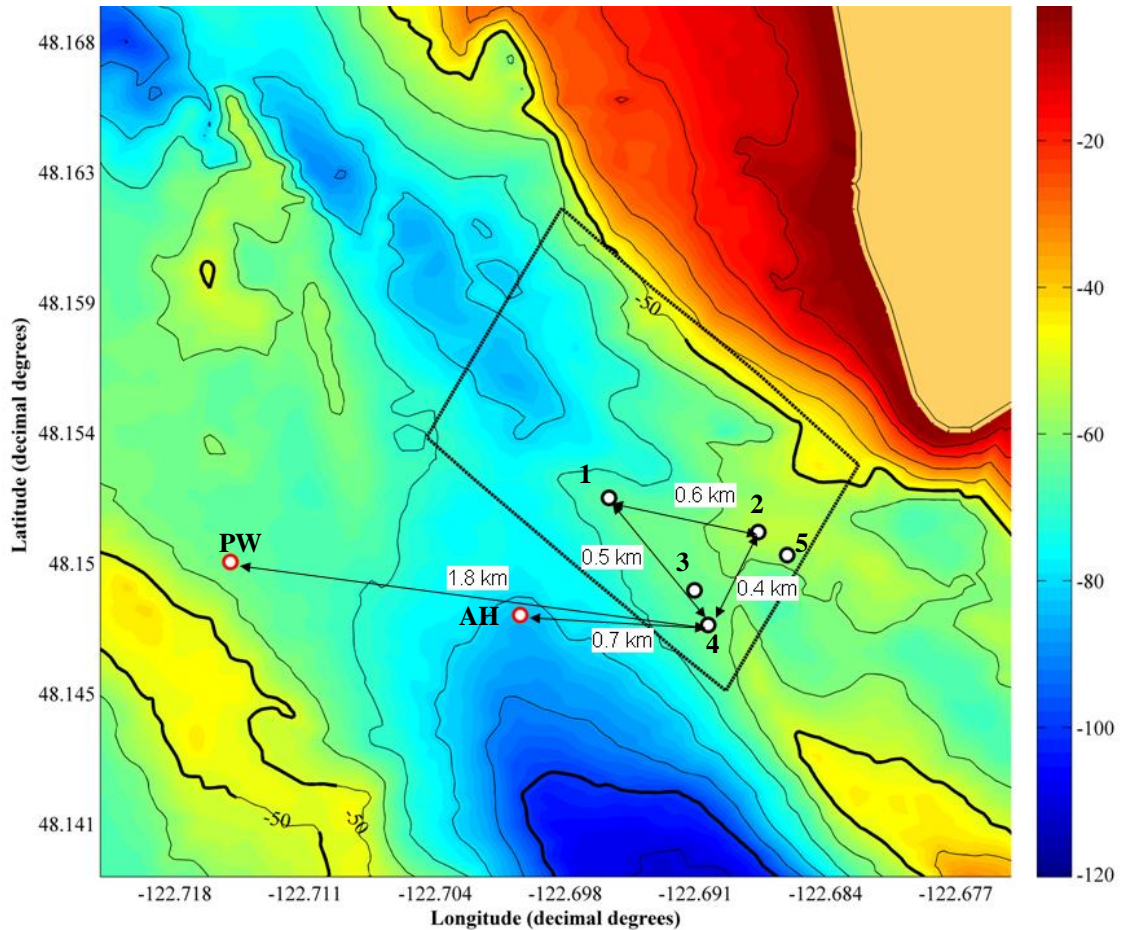


**Figure 15 – Distances between selected sea spider deployments**

The May-August 09 and February-May 2010 deployments are in closest proximity to Admiralty Head, where topography causes a local intensification of the currents. Mean speed, maximum sustained speed, and mean power density are higher at this location. All sites have an ebb/flood asymmetry in direction but the higher intensity sites have relatively more asymmetry in the kinetic power densities as well.

## 2 Stationary Analysis

This section describes the analysis of the ADCP data from stationary sea spider deployments using harmonic analysis. This decomposes the measurement time series into a set of superimposed, periodic forcings, which can be used to make future predictions of tidal currents. The development of this method since it was first proposed by Godin [14] is outlined. The accuracy of the harmonic method on the data from the Admiralty Inlet site is then assessed.

### 2.1 Literature Review

As described in Section 1, the variations in the orbits of the Earth-Moon and Earth-Sun system give rise to variable tractive forces. These in turn lead to tides and tidal currents. The frequencies of these orbital variations can be described by linear combinations of mean lunar time as well as five astronomical frequencies, as specified by Doodson [4]. Mean lunar time accounts for the longitude of the Moon, Sun, the location of interest, and Greenwich Mean Time (GMT) is a convenience selected by Doodson. Each linear combination of the Doodson numbers comprises a tidal constituent. Doodson [4] generated a basis of 388 constituents to describe the periodic behavior of tides and currents. Since inclusion of all tidal constituents would require an impractically long record length (18.6 years) the effects of these minor constituents are grouped with more prominent constituents in the form of a cluster. A cluster of tidal constituents consists of all tidal constituents with the same first three Doodson numbers. The cluster takes the name of the constituent with the largest tidal potential amplitude and all other constituents are termed satellite constituents.

**Table 2 – Lunar Time and Astronomical Variables Developed**

Description	Symbol	Period
Mean Lunar Time	$\tau$	24.8 hrs
Mean Longitude of the Moon	s	27 days
Mean Longitude of the Sun	h	1 yr
Mean Longitude of the Lunar Perigee	p	8.85 yrs
Negative of the Longitude of the Moon's Ascending Node	n'	18.6 yrs
Mean Longitude of the Solar Perigee	p'	21,000 yrs

Constituents classified as astronomical (45 total) are due purely to gravitational forcing. The remaining constituents are referred to as shallow water constituents and are the product of non-linear interactions between the astronomical constituents in shallow water. Using traditional harmonic analysis, tides are described as the superposition of multiple constituent contributions of sinusoidal form that characterizes differences in frequency, phase relative to other constituents, and amplitude. Once a set basis of tidal constituents has been chosen to implement the tidal height harmonic analysis, a least squares solution is found using the following equation

$$y(t_i) = C_0 + \sum_{j=1}^M A_j \cos[2\pi(\sigma_j t_i - \phi_j)].$$

Because the period of the constituents is known *a priori*, a least-squares approach can be used to select the phase and amplitude of each constituent in the series in order to best describe the tidal signal. Once these are established, forecasts and hindcasts of the tides are possible. The five main tidal constituents and their periods are below in Table 3. The type of tidal regime (diurnal, semidiurnal, mixed) is given by the ratio of the primary diurnal amplitudes (O1, K1) to semi-diurnal amplitudes (M2, S2). As this ratio approaches zero, the tidal regime becomes purely semi-diurnal.

**Table 3 – Tidal Constituents Ranked by Tidal Potential, Boon [1]**

Constituent	Name	Period
M2	Main Lunar Semidiurnal	12.42 hours
S2	Main Solar Semidiurnal	12.00 hours
N2	Larger Lunar Elliptical Semidiurnal	12.66 hours
K1	Lunar-Solar Declinational Diurnal	23.93 hours
O1	Lunar Declinational Diurnal	25.82 hours

Godin (1972) [14] developed methods to analyze tidal heights, currents, gravitational acceleration, and other geophysical data series. Godin found that harmonic methods and the more complicated response method of Munk and Cartwright [21] performed comparably when applied to tidal height observations. Due to the comparable performance of the methods as well as the complexity of using the response method, it never gained widespread acceptance like harmonic analysis. From the harmonic analysis method described by Godin, Foreman (1977) [8] created a computational program for tidal height analysis and prediction. The initial program was for a tidal height data series of hourly observations and used a package which attempted to resolve 69 tidal constituents (all astronomical and 24 shallow water) for the time series, as well the option to include up to 77 additional shallow water constituents as specified by the user.

The ability to resolve each tidal constituent depends on the constituent amplitude relative to noise in the measurement, length of record, and the inclusion of other constituents with similar frequency. The Rayleigh Criterion provides for a hierarchy of constituent inclusion during harmonic analysis. Based on the guidelines, a constituent of frequency  $\sigma_1$  would be compared with  $\sigma_0$  and if the length of the data series ( $T$ ) was long enough to satisfy the following inequality it would be included in the subsequent harmonic analysis. Values for  $R$  (Rayleigh Constant) are typically 1 but can be defined otherwise.

$$|\sigma_0 - \sigma_1| * T > R$$

Selection of 69 constituents was suggested by Godin at the time of development because of the increased computational expense and unimportance of including all 145. The computation time increases approximately with the square of the number of constituents. For many tidal height stations, the effects of the shallow water constituents were insignificant and could be left out from the default constituent package, but with capability for manual inclusion [8]. From the criterion, each constituent has a Rayleigh comparison constituent which serves as the basis to determine inclusion. Comparison pairs are defined for each group; the sub-tidal, diurnal, semi-diurnal, and ter-diurnal and determined by the following set of guidelines:

1. Selection based on the magnitude of the tidal potential amplitude, constituents with the largest tidal potential amplitudes in each group are automatically included;
2. Comparisons are made with the constituent closest in frequency which has already been included; and
3. Two constituents which are nearly equal in tidal potential and close in frequency can be included instead as a new representative constituent which will serve as a basis for further inference.

Cases where the criterion fails or performs poorly are common and a series of constituent inclusion charts can be found in Appendix 1. For example, the K1 and P1 astronomical constituents are so close in frequency that a record approximately 6 months long is needed to include both by the criterion.

K1, *Luni-solar diurnal constituent*,  $\omega = 0.04178075$  cycles / hr

P1, *Solar diurnal constituent*,  $\omega = 0.04155259$  cycles / hr

$$|\omega_{K1} - \omega_{P1}| * T > 1 \rightarrow T \approx 182 \text{ days}$$

Shallow water constituent inclusion is based on a ranking of importance by Godin and is included in Appendix 2.

Even an analysis that includes all 145 tidal constituents still neglects long-term variations which would require multiple years of record to include. As discussed previously, constituents are actually clusters of similar Doodson harmonics. That is to say, the amplitude and phase of the “constituent” is actually the amplitude and phase of a cluster containing the main and satellite constituents. Godin applied “nodal corrections”, or more accurately “satellite corrections” to account for the variations in the clusters over time scales longer than a year. Nodal corrections refer to correcting for variations in the Moon’s ascending node  $n'$  only and not the lunar and solar perigees  $p$  and  $p'$ . Godin’s method however did incorporate the variation in the lunar and solar perigees [11]. From the least squares fitting of both tidal heights and currents, the ability to make predictions is also incorporated in the Godin’s method by using the amplitude ( $A$ ), phase ( $g$ ), astronomical argument ( $V$ ), as well as the satellite corrections ( $f$  and  $u$ ) to the constituents used for the prediction period. For tidal heights, the prediction equation is given below (for horizontal tidal currents there is a similar representation):

$$h(t) = \sum_{j=1}^M f_j(t) A_j \cos[2\pi(V_j(t) + u_j(t) - g_j)].$$

For very short record lengths, the Rayleigh Criterion can exclude constituents which are extremely influential in the geographic location. However, this limitation can be overcome by inferring the amplitude and phase of the lesser constituents which do not satisfy the criterion if the constituent has been resolved in the analysis of a longer time series from a nearby site. This requires the assumption that the relative difference in phase and amplitudes of the two constituents be approximately constant across the distance between the two sites. Specifying the ratio of amplitude and difference in phase of a constituent may provide a better characterization of the tidal behavior of the site and is a final improvement to a harmonic analysis [11]. Inference can reduce the residual between the data and the least-squares fit as well as removing periodic behavior in the amplitudes and phases of resolved constituents. The best basis for inference is longer records at the same location, secondly data records from a nearby location, and lastly tidal potential theory [11].

There are limitations to the harmonic method proposed by Godin which must be considered while implementing analysis. During a harmonic analysis, the amplitudes and phases of the included tidal constituents are assumed to be constant over the record which neglects other physical factors such as effects from constituents which are still unresolved after inference or seasonal circulation. Using shorter length of records, a user can circumvent this problem. However there is a trade-off between resolving a greater number of constituents to characterize the site and having a record length without substantial changes in the constituent amplitudes and phases.

Godin's method for tidal height analysis is transferable to tidal current analysis, which decomposes the currents into north/south and east/west components, as explained by Foreman [9]. To simplify the method, the two components are represented as a complex number with the real part being east/west and the imaginary part as north/south. Eastern and northern flows are considered positive for sites on the US west coast. With this representation, the scalar methods developed for tidal heights can be implemented for a complex velocity time series. The use of inference for tidal currents is preferred from historical tidal current records. Using tidal height records for inference requires the assumption that amplitude ratios and phase differences are equal for tides and currents. This can be problematic because of uncertainty in the tidal height/tidal current relationship. As for tidal heights, tidal currents are represented as a series of superimposed sinusoids and, again, a least squares solution is found to:

$$Z(t) = X_0 + \sum_{j=1}^M X_j \cos[2\pi(\sigma_j t - \phi_j)] + i \left[ Y_0 + \sum_{j=1}^M Y_j \cos[2\pi(\sigma_j t - \phi_j)] \right].$$

Tidal currents may be visualized using a tidal ellipse which treats the current signal as a sum of ellipsoids (one for each constituent) instead of a sum of sinusoids. The tidal ellipse is seen below in Figure 16 and has a major and minor axis as well as major axis orientation along with phase lag.

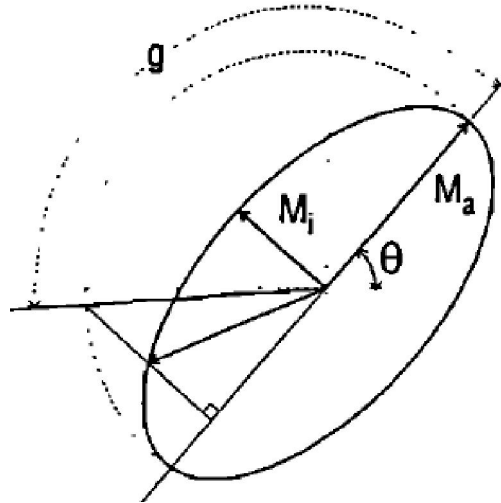


**Figure 16 – Tidal Ellipse for a tidal constituent with major/minor axis amplitude  $M_a$  and  $M_i$ , orientation  $\theta$ , and phase lag  $g$ . Source: Foreman et al. [11]**

Another consideration with harmonic analysis of tidal currents is that tidal ellipse formulation requires that the actual current response from each constituent at a site trace out an ellipse over a tidal cycle (ebb and flood). In near-shore regions, the local bathymetry may cause ebb and flood currents to be asymmetric. Godin [15] proposed using current roses, stick vector diagrams, and progressive vector diagrams to determine when currents are actually elliptical. The ellipses themselves may be near bi-directional and still yield a valid 2D solution, but, for example, if currents rotate in opposing directions between flood to ebb and ebb to flood, 2D solutions are not appropriate, as they rely on a progressive current vector.

In 2002, Pawlowicz et al. [23] ported the FORTRAN package developed by Foreman [8] into MATLAB, a more modern suite of scientific computing tools. The harmonic analysis implemented by Pawlowicz is identical to Foreman's, with the exception that analysis of tidal height and tidal current time series are unified by representing currents as a complex variables. A new development in this package is the generation of confidence intervals for constituent amplitudes and phases by estimating the variance from a spectral analysis on the residual between the harmonic fit and the time series and using a non-linear bootstrapping technique to estimate the errors. Spectral analysis identifies how the total variance in time series is distributed over specified frequencies allowing identification of the dominant periods of variation in the time series. Pawlowicz's spectral analysis uses windows (width 0.4 cycles per day) centered on frequency multiples of the M2 constituent. For example, to estimate the error for M2 (window centered on the M2 frequency) all frequency bins with the exception of the bin containing the M2 frequency are averaged to estimate power (variance) in the

residual Pawlowicz et al. [23]. These estimates of error are then used with standard 95 % confidence interval methods to estimate the error of the amplitude and phase of each constituent. A signal to noise ratio (SNR) is generated and can be used to exclude constituents with unacceptably high noise (subjective). Constituents which pass the Rayleigh Criteria sometimes have extremely low SNR values and subsequently are discarded from the least squares fit. The SNR is defined below with the amplitude  $A$  and the 95 % confidence interval estimate  $\sigma$ .

$$SNR = \left( \frac{A}{\sigma} \right)^2$$

Further improvements Pawlowicz's package have been made by Leffler and Jay [18] who use robust fitting to improve on the ordinary least squares fit by resisting broad spectrum noise. Using an Iteratively Reweighted Least Squares Algorithm, the confidence intervals for the amplitude and phase are reduced, therefore allowing more constituents to meet the significance criteria defined above. To date, this method has only been applied to tidal height time series and future work could investigate the feasibility of using this package for harmonic analysis of tidal currents.

The National Oceanic and Atmospheric Administration (NOAA) generate tidal height and current predictions for many locations around the United States, including Admiralty Inlet. These predictions are used extensively for navigation purposes but when ADCP velocities are compared to NOAA predictions, differences in amplitude and phase are pronounced, as shown in Figure 17. Consequently, estimates of power generation based on NOAA current predictions may be quite inaccurate.

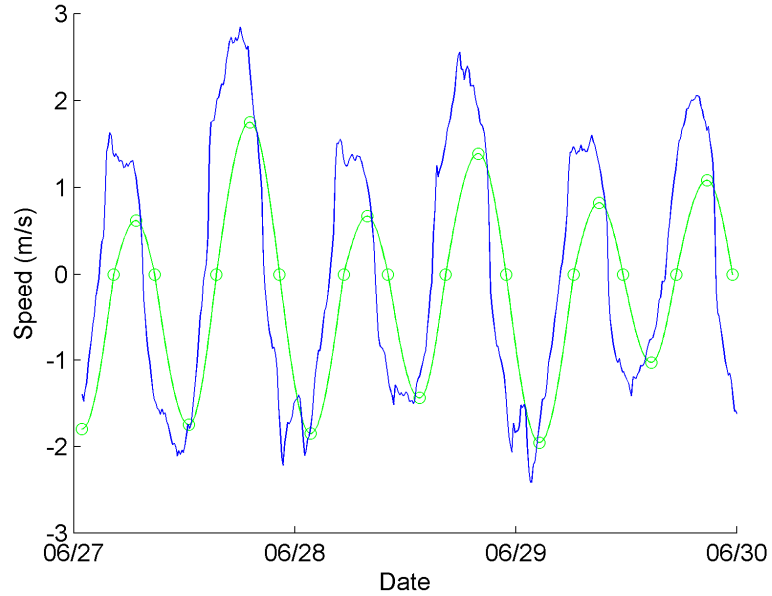


**Figure 17 – NOAA Tidal Current Predictions from Admiralty Head Station (green) vs. ADCP (10 min average, mid water column depth) data from May-August 2009 ADCP Deployment.**

In Figure 18, the difference in timing of slack water near the surface between ADCP measurements and NOAA predictions is characterized for the entire May-August 2009 deployment. For reference, the NOAA prediction station is approximately 680 m west of the August-November 2009 stationary sea spider deployment.

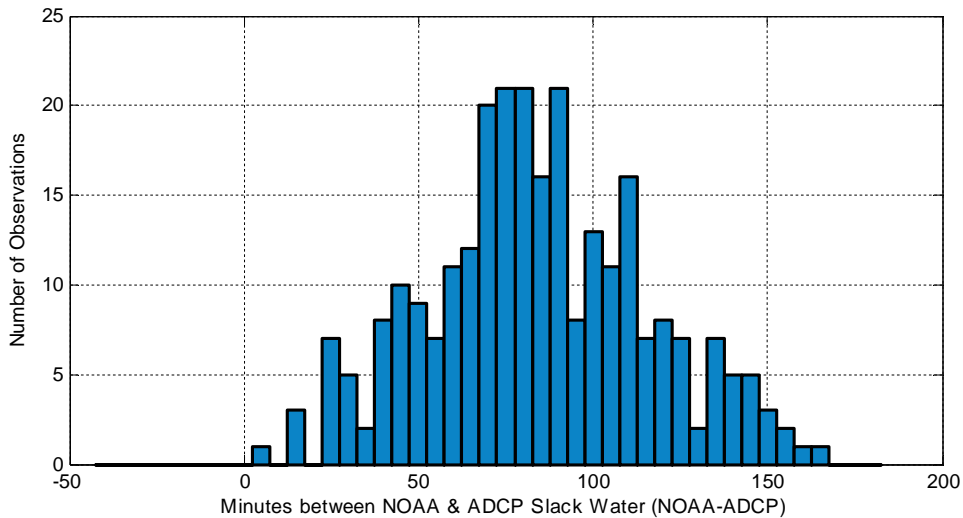


**Figure 18 – Histogram of differences between NOAA slack water timing for the Admiralty Head station and ADCP slack water timing for entire May-August 2009 deployment.**

## 2.2 Methodology

Tidal currents and current structures depend on the response of a particular site to the astronomical forcing. This response may include elements driven by local bathymetry, turbulent eddies, and gravitational circulation due to density stratification. Consequently, while the forcing is largely deterministic, the same cannot necessarily be said of the response to that forcing. This is an important distinction for tidal energy projects since the prediction of the currents will be critical for accurate estimations of the power generated by tidal turbines at the site and the stresses placed on the tidal turbines.

The purpose of these surveys is to gather data which may be used to make an accurate tidal current prediction. Each ADCP deployment has a somewhat different configuration, in an ongoing attempt to optimize data quality and utility against limited power and data storage. The main differences between the deployments have been the time per ping, number of pings per ensemble, and the ensemble interval. Time per ping is the temporal spacing of pings within the ensemble, and pings per ensemble are the number of pings which were averaged for each ensemble interval. Because of memory limitations, individual pings cannot be stored on board the instrument.

**Table 4 – Stationary Tripod Deployments: ADCP properties**

<b>ADCP Properties</b>	April-May 09	May-Aug. 09	Aug.-Nov. 09	Nov.-Feb. 10	Feb.-May 10
Depth (m)	65.0	53.7	63.3	62.7	57.1
Record Length	40.3 days	75.2 days	98.8 days	72.6 days	82 days
Acoustic Frequency	307.2 kHz				
Time / Ping	8.57 sec	0.57 sec	2.25 sec	0.56 sec	0.57 sec
Vertical Bin Size	1.0 m	1.0 m	1.0 m	1.0 m	1.0 m
Pings / Ensemble	70	16	60	22	26
Ensemble Interval	10 min	30 sec	135 sec	45 sec	60 sec
Blanking Distance	1.76 m				

The data collected by the ADCP goes through post-processing to further assure the quality of the record. During this process, velocity measurements shadowed by reflection from the free surface are removed from the record. The approximate shadowing distance ( $h_s$ ) is given by Brown et al. [2]

$$h_s = H(1 - \cos \phi),$$

Where  $H$  is the water depth and  $\Phi$  is the ADCP transducer angle measured relative to vertical ( $20^\circ$ ). Because the instrument being used for these studies does not have an integrated pressure sensor, the free surface elevation is estimated by aligning the output of a separate pressure sensor (accurate for change in elevation, but significant error in absolute depth of order 1m) with the ADCP backscatter intensity maxima. Additionally, adjustments are also made to account for the height of the transducers above the seabed and daylight savings time.

There are a number of possible approaches for extracting tidal constituents from a current record – each involving trade-offs. In all cases, the vertical component of velocity is neglected [1] and tidal constituents are evaluated for each depth bin. Three approaches for the horizontal velocity field are:

1. *UV components*: treating the currents as a complex progressive vector (i.e., an ellipse);
2. *Principal axis*: reducing the problem to a single dimension by evaluating only the component of the horizontal velocity parallel to the principal axis (i.e., the axis describing the maximum variance in the time series), and dismissing velocities perpendicular to the principal axis as non tidal behavior; or
3. *Signed speed*: reducing the problem to a single dimension by calculating the current speed as the vector average of the two horizontal components and signing flood currents positive and ebb currents negative (as defined by the principal axes).

In the interest of brevity, results are presented for currents measured in the middle of the water column. These are also the “cleanest” tidal current measurements since close to the surface currents include non-tidal forcing from weather and close to the bottom currents are more strongly influenced by bathymetry.

Prior to applying any of these methods, further ensemble averaging of the time series may be useful to remove high frequency noise (e.g., turbulence) from time series visualizations. Figure 19 shows the difference between the raw ADCP data (ensemble average of 2:15) and a longer post-processed ensemble (20:15). It is apparent that the raw ADCP data has a degree of noise in the signal and when further averaged the noise is smoothed out and reduced. Note, however, that even with this degree of averaging, the currents do not resemble a smoothly varying sine wave.

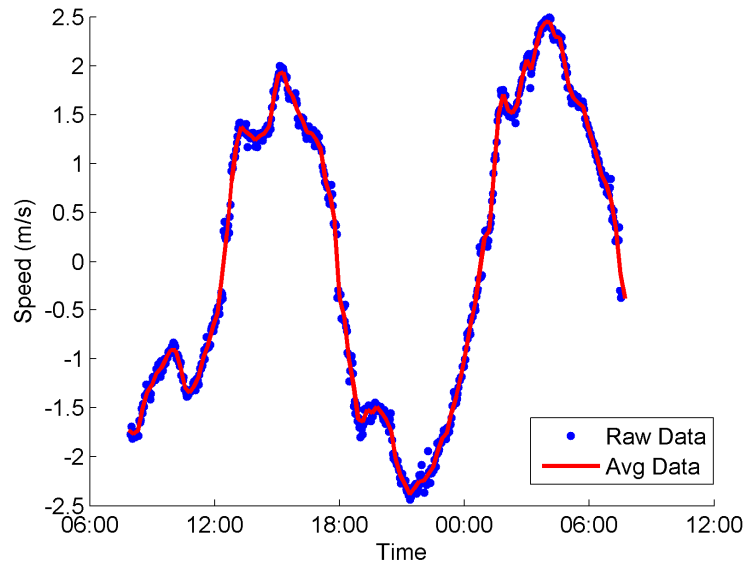


**Figure 19 – Comparison of raw ADCP data vs. post averaged data, mid water column velocities**

Two dimensional current analysis (UV components) implements a complex harmonic analysis, permitting the use of scalar methods by keeping each velocity component in either real or imaginary space. When using UV components, the harmonic analysis will find not just an amplitude and phase for each tidal constituent, but a major and minor amplitude and phase for each constituent. These parameters make up the tidal ellipse for each constituent and through superposition they can be recombined to fit the observations or make a prediction. Tidal ellipse methods assume that both the ebb and flood are axis-symmetric (e.g., major axis  $180^\circ$  out of phase) and that the ellipse for a single constituent rotates only clockwise or counter-clockwise as it progresses from ebb to flood.

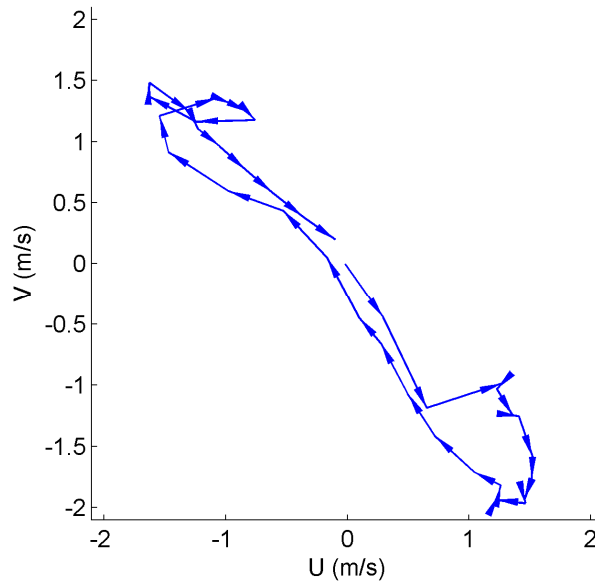


**Figure 20 – Path traced out by tip of current vector over one tidal cycle (9/18/2009, 10:30-22:40). Blue is averaged ( $\approx 20$  min, mid water column depth) data**

Seen above in Figure 20, near the peak flood current, the averaged data follows a largely elliptical path until around peak ebb when both magnitude and direction become more erratic. The progression of the tidal ellipse shows a distinct jump in direction as the ellipse progresses towards peak flood and then towards peak ebb. Fitting two dimensional currents does have a distinct advantage over the other two methods discussed in that none of variance in the tidal currents is lost prior to harmonic analysis. However, particularly around the time of peak currents, the fundamental assumptions required for two dimensional analyses are violated to a degree.

Principal axis currents are simply a rotation of the northerly and easterly velocity components which are recorded by the ADCP. The rotation is accomplished by projecting all two dimensional velocity vectors in the time series onto two new orthogonal axes which have the same variance as the original series. The variance along the principal axis however represents the maximum fraction of total variance, while the minor axis accounts for any remaining variance. Below in Figure 21 is the principal axis rotation of mid water column velocities for the August through November 2009 deployment.

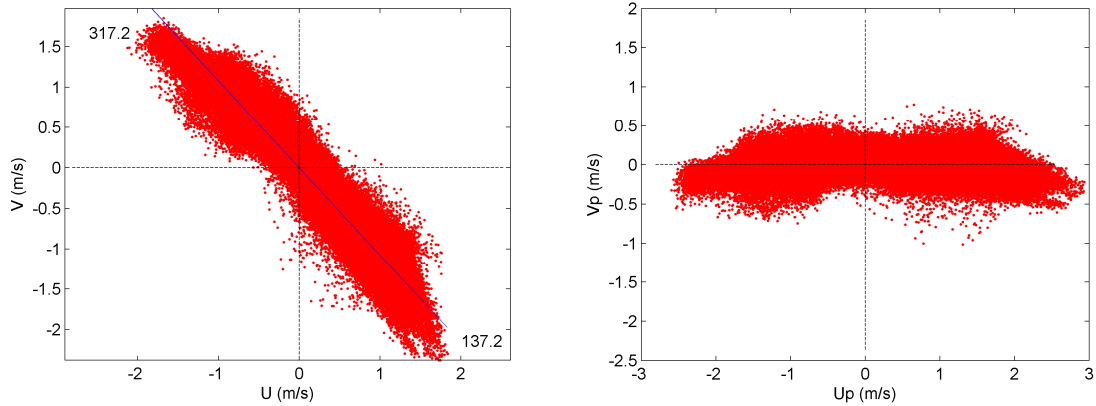


**Figure 21- Principal axis rotation, U and V are east and north velocity, Up and Vp are principal and minor axis velocities, principal axis variance = 97.4% of total variance, principal axis heading 137.2° for ebb and 317.2° for flood (true north = 0°, clockwise positive).**

Principal axis currents reduce the dimensionality of the currents from two to one, but care must be taken when neglecting the minor axis velocities. If currents are significantly elliptical or directionally asymmetric, then the discarded variance along the minor axis may contain important information. Turbulent fluctuations in velocity are projected on to both axes but, ideally, are preferentially captured by the minor axis. At sites which experience nearly bi-directional currents, the use of principal velocities represents most if not all of the periodic variation in the currents and can be a useful tool to simplify the analysis.

Using a signed speed for analysis also preserves the variance in the original time series and, unlike principal axis analysis, can account for tidal currents with substantial (e.g., > 10 degree) directional asymmetry between ebb and flood. Signed speed is the magnitude of the currents while using the principal axis to determine ebb (negative sign) or flood (positive sign). Signed speed is representative of the maximum power density or maximum power generation (when combined with efficiencies) that a hydrokinetic device could remove from a flow, provided that the turbine can remain aligned with the direction of the flow.

### 2.3 Results & Discussion

The stationary ADCP analysis compares the performance of harmonic analysis methods when using principal axis, two-dimensional, or signed speed as an input. Due to the advantages and limitations of

the three previous representations, the analysis is used to identify which velocity representation results in the best prediction of the currents. It is completely possible however that for sites with strong tidal currents that there may be no statistically better approach (i.e., a site could have asymmetrically oriented ellipses). *t\_tide* measures quality of the harmonic fit (superposition of sinusoids, 1 for each constituent) to the data based on variance in the fit relative to the total variance. Other measures of quality, such as predictions of peak current or slack water timing are not captured in variance comparisons and must be evaluated separately. For example, a harmonic prediction 90° out of phase with the input time series could have the exact same variance, but would be an exceptionally poor prediction.

The *t\_tide* harmonic analysis package has the option to include inference for constituents which would otherwise be excluded by the Rayleigh Criterion (2.1) due to the length of the record. Inference uses an amplitude ratio and phase adjustment between a primary constituent and the next largest constituent of same diurnal or semidiurnal classification that is not included. However, the amplitude ratio and phase adjustment must be obtained from a data series of sufficient length to satisfy the Rayleigh Criterion and are subject to the further assumption that neither of these factors vary substantially in space between the locations of the two time series. For the purposes of this assessment, the time series from two stationary deployments (August-November 2009 and November-February 2010) were combined to create a representative long-term record which enabled the resolution of a number of otherwise hidden constituents. This requires several assumptions:

1. the currents do not vary substantially between these two deployment locations (~145m in the along-channel direction);
2. the gap in the data series during recovery and redeployment (~1 day) is not significant; and
3. the Rayleigh Criterion may be slightly relaxed to accommodate a time series 172 days in length, rather than 182 days required for strict application.

The experimental plan called for these two deployments to be co-located and run for 190 days, but during the November redeployment, conditions were too rough to manage redeployment in the same location and the ADCP depleted its battery faster than anticipated during the November-February deployment. Because the ensemble interval varies between the two deployments, the November-February measurements are ensemble averaged to the same interval as the August-November series, prior to analysis.

By combining the records, the amplitude and phase of additional constituents can be found resolved. Two important constituent pairs which cannot be resolved by shorter term measurements are P1 from K1 and K2 from S2. K2 and P1 are the largest amplitude diurnal and semi-diurnal constituents excluded by the Rayleigh Criterion for records shorter than 182 days. Below are the harmonic analysis results of amplitude and phase corrections at all water depths using the three different approaches to handling the two dimensional velocity input.

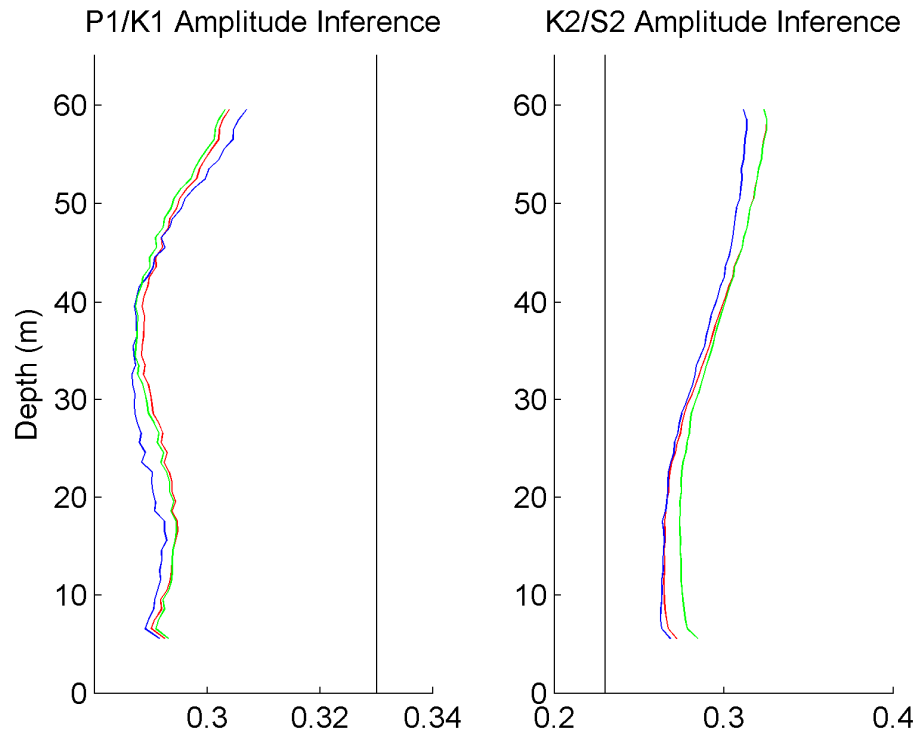


**Figure 22 – Amplitude inference results from long record harmonic analysis of difference velocity sets. Red is for principal axis, blue is for signed speed, and green is for complex. Black is tidal height amplitude ratio from Lavelle et al. [19].**

There is a slight variation in these ratios throughout the water column but the general trend with depth is consistent between the different approaches. Although comparison of inference properties between tidal height (long term records often available) and current is questionable, the ratios seen from the current analysis are not entirely different from those inferred from tidal heights by Lavelle et al. [19], who estimated the P1/K1 ratio to be 0.33 and the K2/S2 ratio to be 0.23 from observations and equilibrium tidal potential theory. The results obtained from current data show the ratio to be smaller than that estimated by Lavelle et al. for the diurnal constituents and larger for the semi-diurnal constituents. The variations in the ratios with depth suggest that application of tidal height records as

inference predictors for tidal current analysis should be used cautiously and only when tidal current series of sufficient length are not available.

Similar results are obtained for tidal current phase inference of P1 and K2. As shown in Figure 23, there are phase variations of ten degrees (40 minutes) or more through the water column, which is significantly different from the results obtained by Lavelle et al. [19] which found tide phase differences of 2.6 and 1.2 degrees, respectively.

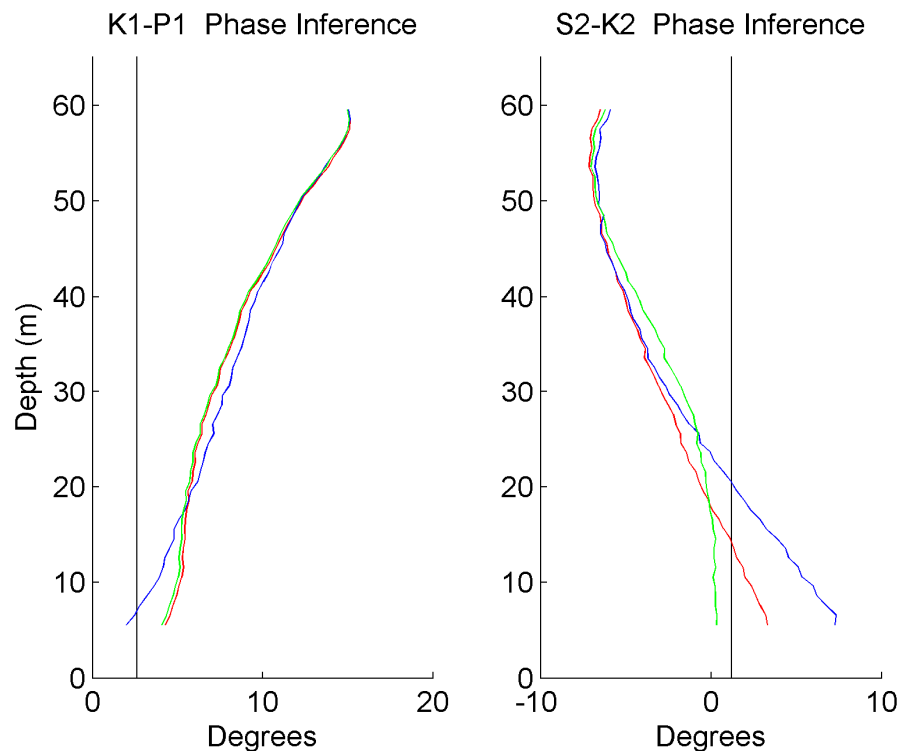


**Figure 23 – Phase inference results from long record harmonic analysis of different velocity sets. Red is for principal axis, blue is for signed speed, and green is for complex. Black is tidal height phase difference from Lavelle et al. [19].**

Due to the complexity of tidal currents, the departure from values estimated from tidal heights and variations with depth are not surprising. This demonstrates that a harmonic analysis of a three month record with inference must not only use inference from previous tidal current analyses but also from the same approximate depth to obtain the most accurate ratios. For the comparison of harmonic analysis, a depth of approximately 10 m was selected, since this is the hub height of the OpenHydro turbines proposed for deployment in Admiralty Inlet. Since the ADCP did not have a depth bin centered at 10 m, the closest bin closest was used instead. Harmonic analysis with inference is only

applied to the data sets collected from August-November 2009 and November-February 2010 sites. Further work is required to determine if inference ratios vary throughout the survey area. Figure 24 shows a three day window of a representative portion of the tidal cycle with the raw data, harmonic fit, and residual. The inference amplitude ratios and phase differences correspond to signed speed values from Figure 22 and Figure 23. Inference values for the comparison of the different current representations correspond to the values from analysis of the specific representation.

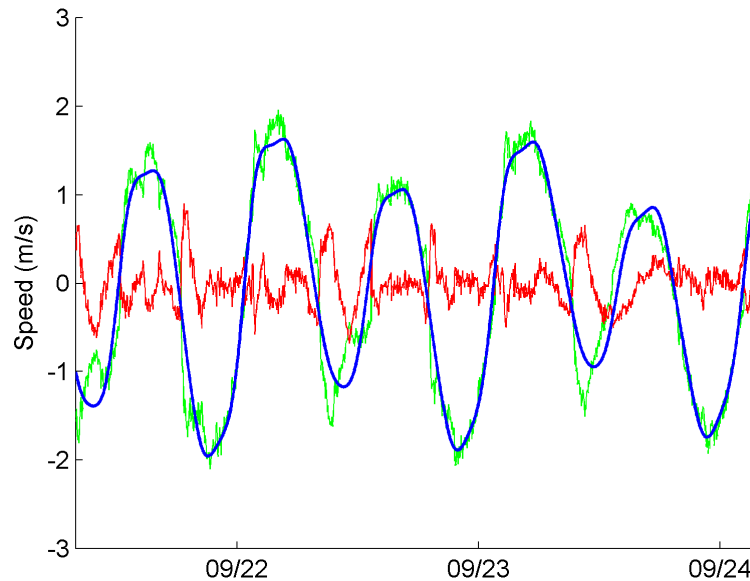


**Figure 24 – ADCP signed speed (green), T Tide harmonic fit to signed speed (blue), residual (red). Inference used for P1 and K2 constituents, water depth (10 m)**

The residual is significant, at times exceeding 0.5 m/s. While the fit follows the trend of the data well, large residuals are present throughout the time series. Residuals are due to differences in current magnitude, current phase, or a combination of the two. This shows that the harmonic analysis of signed speed is unable to approximate the data accurately a significant portion of the time. As previously mentioned, one measure that can be used to evaluate the fit is the total variance in the fit versus total variance in the input time series. It is an important point to realize that variance does not account for differences in phase, just deviations in the data or fit around the mean. This measure is used by the *t\_tide* harmonic analysis package to assess the fit. As shown in

**Table 5**, there are only minor variations in this figure of merit for the three different representations of the velocity.

**Table 5 – Percent Variance Fit by Harmonic Analysis (hub height  $\approx$  10 m)**

ADCP Deployment	Principal Axis Velocity	Complex Velocity	Signed Speed
	<i>var(harmonic analysis) / var(raw signed speed)</i>		
<b>August-November 2009</b>	88.9%	90.7%	95.4%
<b>November-February 2010</b>	87.1%	89.8%	95.6%

A second metric to assess the goodness of fit (amplitude and phase error) is the coefficient of multiple determination (R-squared). Instead of evaluating the relative variance of the harmonic fit and input time series, the R-squared statistic evaluates the proportion of the velocity variation that can be attributed to the resulting harmonic fit [5]. A perfect fit by the harmonic approximation would have an R-squared value of 1. The R-squared value is given by

$$R^2 = 1 - \frac{\sum_i (\hat{y}_i - y_i)^2}{\sum_i (y_i - \bar{y})^2},$$

where  $\bar{y}$  is the mean of the velocity time series,  $y_i$  is each velocity data point in the series, and  $\hat{y}_i$  is the harmonic fit for each velocity data point in the series. The resulting R-squared values indicate that none of the representations for horizontal velocity are superior. A further refinement, excluding points below 1 m/s, indicates that all methods perform somewhat better for stronger currents. This speed is significant because it is the approximate cut-in speed (speed at which the blades begin to rotate) for a tidal turbine. Therefore, low accuracy around slack water does not affect power generation estimates.

**Table 6 – R-squared values for harmonic approximation (hub height  $\approx$  10 m)**

ADCP Deployment	Principal Axis Velocity	Complex Velocity	Signed Speed
	<i>R-squared</i>		
<b>August-November 2009</b>	0.94	0.95	0.94
<b>November-February 2010</b>	0.95	0.96	0.95
	<i>R-squared above cut-in speed of 1 m/s</i>		
<b>August-November 2009</b>	0.97	0.97	0.97
<b>November-February 2010</b>	0.97	0.98	0.98

Harmonic analysis may be unable to approximate the remaining proportion of variation in the data if the residual currents are due to the effects of turbulence, bathymetry, or density stratification. To investigate whether the harmonic analysis removes all the effects of barotropic forcing, the residual can be analyzed by spectral analysis to identify which frequency bands contain variance. Ideally, harmonic analysis should remove most of the energy in the diurnal and semi-diurnal frequencies.

Spectral analysis uses a fast Fourier transform to convert a velocity signal from the time domain to the frequency domain. The range of discrete frequencies resolved by the transform are determined by the Nyquist frequency (highest) and the length of record (lowest). The Nyquist frequency is the highest frequency that can be resolved from a discrete time series and is defined by

$$f_N = 1/2\Delta t,$$

where  $\Delta t$  is the sample time spacing. The length of record determines both the lowest frequency defined as the inverse of the record length as well as the frequency resolution given by  $\Delta f = 1/T$ .

An advantage of spectral analysis is the straightforward identification of energy containing frequencies. Below in Figure 25 is the spectral representation of a signed speed time series and the residual from *t\_tide* harmonic analysis. The frequency range shown (x axis) has been truncated to emphasize the diurnal and semidiurnal bands and does not indicate the Nyquist frequency. To reduce uncertainty in the spectral analysis, a Hamming filter with 17 windows (50% overlap) is used. Windowing increases the degrees of freedom and therefore statistically increases the reliability of the power spectral density.

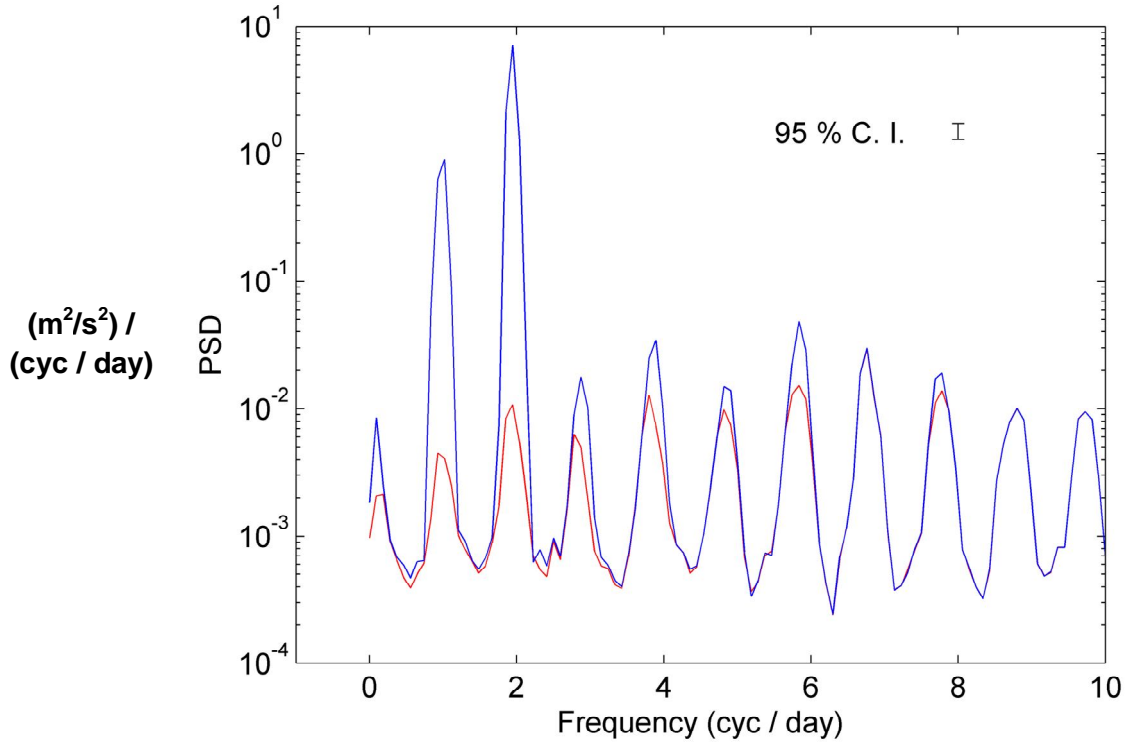


**Figure 25 – Power spectral density of signed speed data (blue) and residual (red) between harmonic fit and data for August-November 2009 deployment and hub height.**

The residual signal in Figure 25 has noticeable peaks in diurnal and semi-diurnal frequencies but the actual amount of the variance removed from those frequency ranges is quantified below in Table 7.

**Table 7 – Signed Speed and Residual Variance in Diurnal and Semidiurnal bands**

Frequency (cyc / day)	Variance		% Variance Remaining
	Signed Speed	Residual	
0.83 - 1.20	0.1539	0.0011	0.74
1.85 - 2.22	0.8707	0.0021	0.24

One challenge to spectral analysis is spectral leakage. Spectral leakage is caused when the fundamental frequencies in the time series are not exactly aligned with a resolved frequency bands (determined by the Nyquist frequency and length of record) but still within the total range. Each neighboring frequency bin which contains some of the energy from the main peak is called a side lobe. Filters, such as the Hamming filter, taper in the initial velocity time series to reduce the magnitude of the spectral leakage. The Hamming filter is designed to reduce the spectral leakage in the lobes surrounding the main lobe (centered on frequency of interest), allowing better resolution of

the small spectral peaks in neighboring frequency bins. Figure 26 shows the Hamming filter operation on a signed speed time series for one of the windows analyzed previously in Figure 25.

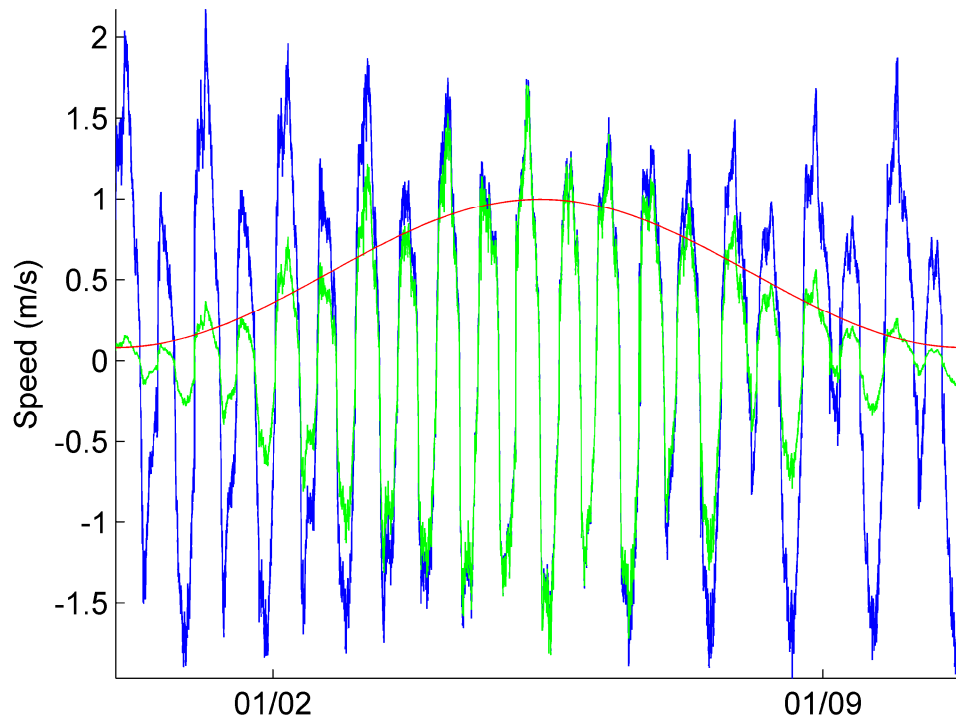


**Figure 26 – Raw Signed Speed Signal (blue), Hamming filter (red), Tapered Signed Speed Signal (green)**

From the plot of power spectral density (Figure 25), it can be seen that the harmonic analysis does remove a considerable portion of the power associated with diurnal and semi-diurnal frequencies. There is still, however, remaining power in the residual which is not resolved by harmonic analysis. One interesting observation is that all the energy containing frequencies have been reduced to a similar order of magnitude. This may suggest a limiting threshold for harmonic fits.

The spatial variability of the currents can be characterized by examining the spatial variation of the tidal constituents which comprise the majority of the total forcing. The M2 tidal constituent has forcing that contributes more to the strength of the currents in Admiralty Inlet than any other constituent, see Table 8. Stationary ADCP deployments separated by only a few hundred meters may have large M2 amplitude variations.

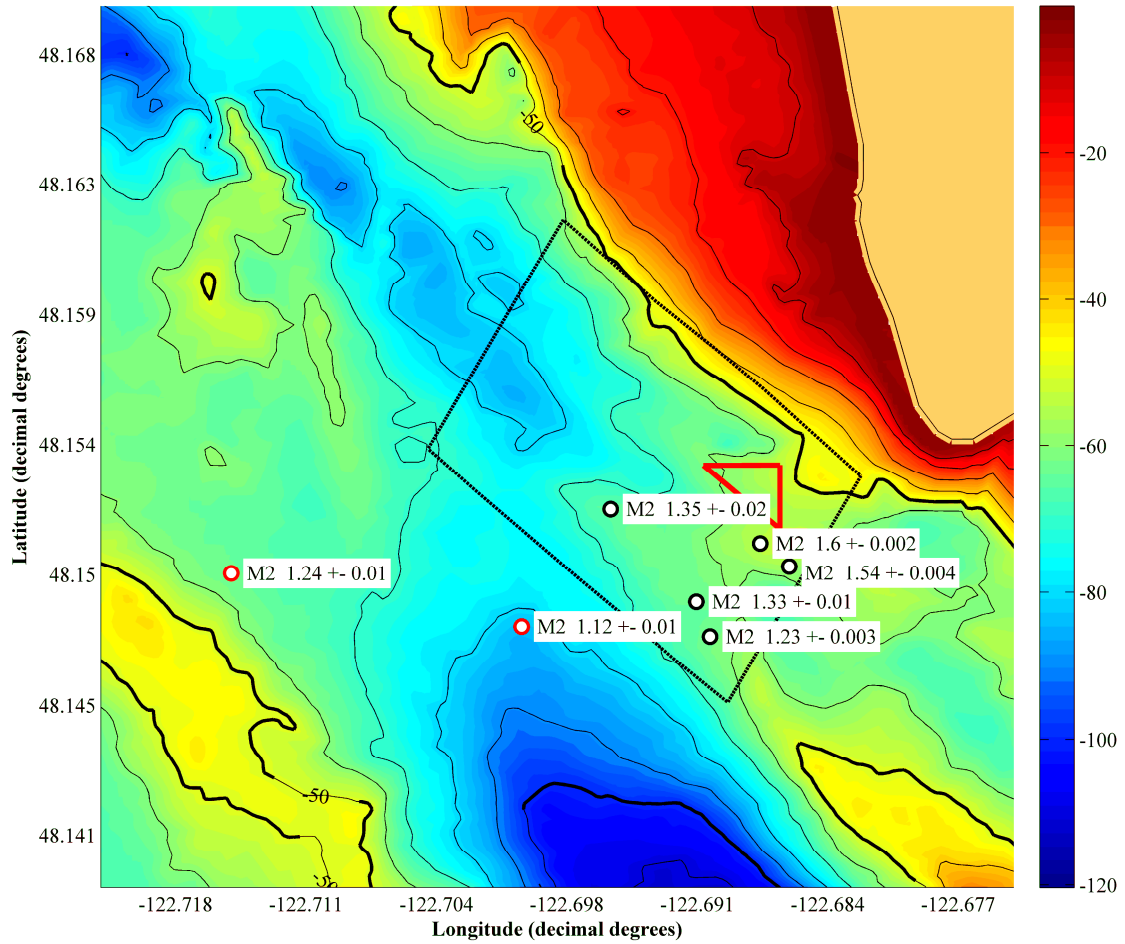


**Figure 27 – M2 constituent amplitude (m/s) from stationary ADCP deployments superimposed over bathymetry (m). Black circles are UW- NNMREC ADCP deployments. Red circles are Evans Hamilton, Inc. deployments.**

M2 phase differences are less pronounced through the area with maximum differences of roughly 5 degrees or 20 minutes. Moving away from Admiralty head there is a difference of almost 15 minutes over a 400 m distance. The variability has both along channel and cross channel variation.

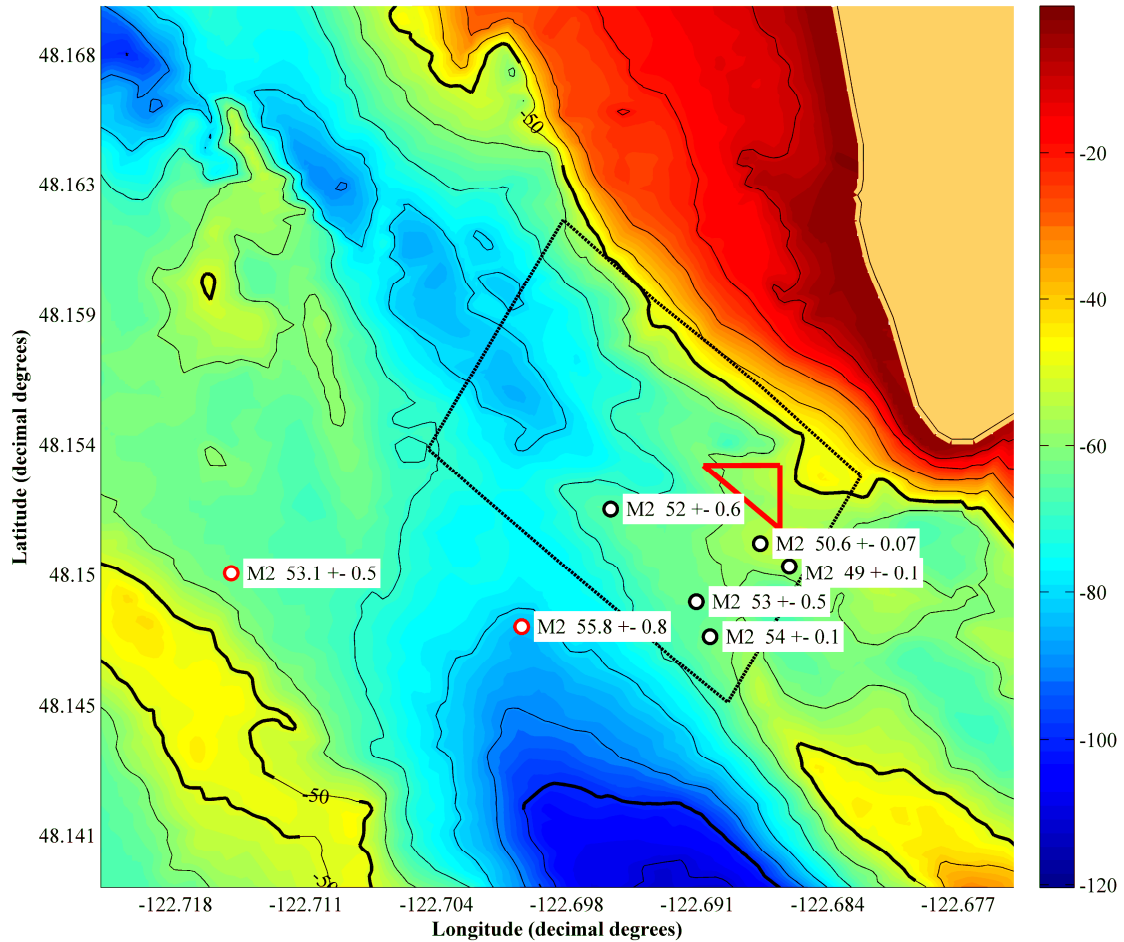


**Figure 28 – M2 constituent phase (deg) from stationary ADCP deployments superimposed over bathymetry (m). Black circles are UW- NNMREC ADCP deployments. Red circle Evans Hamilton, Inc. deployment.**

Amplitude and phase variations for the S2, K1, O1, and N2 tidal constituents are shown in Table 8 and do not include inference for P1 and K2. This is a conservative assumption made for consistency because the inference obtained for the August-February time series may not be appropriate to apply to other measurement locations. The trends in the M2 amplitude are similar to trends with the other constituents with a few exceptions. Both deployments nearest to the headland have the largest two M2, O1, and N2 amplitudes but differences in S2 and K1 amplitudes. Differences in phase across the site range from 7° degrees with M2 up to 36° with K1 and are found between UW NNMREC deployments and Evans Hamilton deployments.

**Table 8 – *t* tide amplitude and phase results with 95% confidence intervals.**

Tidal Constituent	Stationary ADCP Deployment						
	1	2	3	4	5	AH	PW
<b>M2</b>							
Amplitude (m/s)	1.35	1.60	1.33	1.23	1.54	1.12	1.24
Amplitude error (m/s)	1.5E-02	1.9E-03	1.2E-02	2.8E-03	3.7E-03	1.4E-02	1.1E-02
Phase (deg)	51.98	50.64	52.96	54.02	49.00	55.78	53.08
Phase error (deg)	0.61	0.07	0.50	0.15	0.12	0.77	0.53
<b>S2</b>							
Amplitude (m/s)	0.37	0.29	0.39	0.25	0.51	0.41	0.43
Amplitude error (m/s)	1.5E-02	1.7E-03	1.2E-02	2.6E-03	3.4E-03	1.3E-02	1.1E-02
Phase (deg)	53.03	72.42	60.93	72.39	63.57	83.09	84.12
Phase error (deg)	2.44	0.37	1.60	0.59	0.35	2.16	1.24
<b>K1</b>							
Amplitude (m/s)	0.52	0.70	0.42	0.59	0.47	0.35	0.37
Amplitude error (m/s)	1.1E-02	3.1E-03	1.0E-02	5.7E-03	9.5E-03	8.1E-03	4.9E-03
Phase (deg)	51.72	70.20	68.12	66.22	62.90	87.41	87.30
Phase error (deg)	1.19	0.31	1.30	0.52	1.29	1.22	0.66
<b>O1</b>							
Amplitude (m/s)	0.25	0.30	0.27	0.24	0.30	0.27	0.25
Amplitude error (m/s)	1.1E-02	3.2E-03	7.9E-03	5.7E-03	1.1E-02	8.5E-03	4.1E-03
Phase (deg)	51.29	60.56	53.14	53.53	50.43	70.66	65.24
Phase error (deg)	2.39	0.61	1.72	1.36	1.97	1.66	1.13
<b>N2</b>							
Amplitude (m/s)	0.23	0.35	0.24	0.23	0.34	0.24	0.27
Amplitude error (m/s)	1.4E-02	2.0E-03	1.1E-02	2.8E-03	3.3E-03	1.4E-02	1.1E-02
Phase (deg)	30.90	26.55	14.47	34.68	12.17	32.37	45.52
Phase error (deg)	3.50	0.30	3.31	0.70	0.57	3.46	2.18

Variability over length scales less than 100m could be resolved with additional stationary ADCP deployments, but only at high cost. An alternative, discussed in Section 3, is the use of shipboard ADCP surveys to resolve variations in current amplitude and phase. These surveys, however, do not resolve individual constituents, only the amplitude and phase of the tidal cycles which are included in the survey.

Future research could focus on analysis of residual currents and the possibility of using empirical orthogonal functions (EOFs) to further quantify the residual between harmonic analysis and the underlying time series. EOFs use inverse methods to represent spatial and temporal variability in terms of orthogonal functions or statistical modes [6]. Additional stationary ADCP deployments will

also provide a longer record from which to resolve inference characteristics of tidal constituents which are discarded by the Rayleigh Criterion. From the approximations of the tidal currents at Admiralty Inlet it can be concluded that the process is not completely deterministic and contains a combination of bi-directional and elliptical flow from which no one method of characterization outperforms the others. Better understanding of the flow interactions with the sill, bathymetry, and headland could also lead to insight on how to better predict current velocity.

### **3 Mobile Analysis**

For the siting of marine hydrokinetic energy devices, it is very important to resolve relatively small variations in both peak currents and the timing (phase) of peak. The power density of tidal currents scale with the velocity cubed. Small increases or decreases in velocity alter the power a device can generate from the flow and would be extremely important for commercial scale projects. Previous work with shipboard ADCPs has implemented detiding techniques on spatial scales of about 1 km or served as a merely qualitative tool in identifying regions of strong currents. One kilometer resolution is sufficient to identify large current structures and principal flow directions but is not fine enough to optimally site a tidal turbine. Analysis of stationary ADCP data collected in Admiralty Inlet (Table 1) indicate differences in the mean power density on the order of 47% of max mean power density due to major tidal constituent amplitude and phase variation in the survey area.

As discussed in the previous chapter, because of the large spatial variations in tidal currents in northern Admiralty Inlet, the variability cannot be realistically resolved through the use of stationary ADCPs and subsequent interpolation. Shipboard surveys provide a lower effort solution to resolving tidal currents through either harmonic analysis of survey tracks or the assimilation of tidal current models and stationary data with observations.

#### **3.1 Literature Review**

Ship mounted ADCPs are a long practiced use of the technology. Initial use of data collected in this manner was limited due to inaccuracies associated with separating the ship's velocity from currents. Improvements in the late 1980s resolved this issue with the incorporation of bottom tracking capabilities which could separate ship speed from water velocity with higher confidence. The advantage of ship-mounted ADCP surveys are the measurable spatial variations in current or current structure that singular stationary deployments or interpolations between deployments are unable to resolve.

A ship mounted ADCP was used to measure the currents through the Minch between Scotland and Herbides by Simpson et al. [26]. Transects across the channel were approximately 20 km. Vertical resolution of 8 meters and horizontal resolution of approximately 1 kilometer (4 minutes temporally)

were successful in mapping the flow through the Minch from two separate ship surveys of 11 and 12.5 hours in February 1988. The least-squares analysis used a sinusoidal representation of the M2 semi-diurnal constituent to fit the depth averaged current  $u(t)$ .

$$u(t) = A \cos(\omega t + \phi) \rightarrow u(t) = A \cos(\omega t) + B \sin(\omega t)$$

The S2 constituent was then included based on an amplitude correction of the M2 amplitude and phase from a two-component tidal signal model. By estimating and separating the effects of S2, the phase of M2 across the channel was then found. The survey period was not long enough to resolve any of the diurnal variation at the channel, though diurnal tides are relatively weak in that area of the world and unlikely to confound survey results. The M2 amplitude and phase found across the Minch was in agreement to a 3-D regional model by Proctor and Wolfe [25]. This work served as an early demonstration of the potential for shipboard ADCP surveys.

Geyer and Signell [13] used ADCP surveys around Gay Head in Massachusetts with a similar fitting method as Simpson et al. to map tidal current structure. Peak currents at Gay Head are less than 1 m/s and dominated by the M2 semi-diurnal tidal constituent. Survey duration was about 12 hours and each of the 8 cruises between February and June 1988 ran 1 of 5 different survey track orientations. The 5 survey tracks were trapezoidal with overlapping edges, mapping both sides of the headland. Each lap was 10 km long and required about 1 hour to complete ( $\sim 3$  m/s vessel speed). The track was divided into 200m bins, creating a time series of measurements over the survey duration at each bin along the track. A harmonic analysis was implemented for M2, as well as the M4 and M6 over-tides to the observations, allowing the tidal flow field around the headland to be resolved within 5 cm/s. The different surveys were compared by using a normalization which applied an amplitude factor and phase shift to each data set which depended on the tidal characteristics of the site during the survey. By normalizing the individual cruises, Geyer and Signell showed that observations from different surveys spanning five months showed consistency.

A second method to resolve the spatial resolution of tidal currents from shipboard surveys was developed by Candela et al. [3] and used only one survey spanning five days with no repeat of any transect. This survey took place in the Yellow Sea. This differs from the previously described methods which aim to build up a time series of tidal currents in each horizontal bin of a lap. The total survey area of 300km by 500km was binned into 20km segments along the ship's track. For surveys of this spatial scale, repeat transects would have been impractical. Along each segment, measured

currents were averaged temporally, spatially, and vertically into 10m depth bins. The standard form of the equation for current observations

$$u(t) = u_o + \sum_i^n a_i \cos(\omega_i t - \theta_i),$$

can be expressed instead as

$$u(t) = u_o + \sum_i^n A_i \cos(\omega_i t) + B_i \sin(\omega_i t),$$

where transformations back to amplitude and phase are given by

$$a_i = \sqrt{A_i^2 + B_i^2} \quad \& \quad \theta_i = \arctan\left(\frac{B_i}{A_i}\right).$$

A least-squares analysis was used to fit the data, and Candela et al. instead described with the amplitudes and phase of the M2 and K1 partially prescribed as a function of spatial position (mean flow component not shown).

$$u(x, y, t) = u_o(x, y) + \sum_i^n A_i(x, y) \cos(\omega_i t) + B_i(x, y) \sin(\omega_i t)$$

$$A(x, y) = \sum_j \alpha_j f_j(x, y)$$

$$B(x, y) = \sum_j \beta_j f_j(x, y)$$

For each of  $n$  constituents, the amplitude of both terms are defined as a functions of spatial location (x and y) and the least squares solution varies both  $\alpha$  and  $\beta$  for tidal constituent  $i$ . By selecting only M2 and K1 constituents ( $i=2$ ), all the semi-diurnal and diurnal variation was concentrated into the M2 and K1 amplitude and phase estimates. Mean flow was fit with a first order polynomial and  $A(x, y)$  and  $B(x, y)$  for M2 and K1 were fit with second order polynomials. Coefficients of the polynomials or bi-harmonic functions minimize the residual. The use of polynomial and bi-harmonic functions was arbitrary and improvements could be made by using equations more suited to fit the tidal dynamics of the individual site. Resulting from the arbitrary use of polynomial and bi-harmonic functions were smooth tidal flows that agreed with tidal charts of the region. This work, like Simpson et al., was aimed at detiding (removing tidal currents) observations prior to further analysis, as opposed to fitting the tidal currents with the intention of resolving constituent amplitudes and phase.

Additional work was performed in the early 1990's around Vancouver Island by Foreman and Freeland [10], who applied two different detiding methods for shipboard ADCP measurements from a 3 day cruise. The first method used a barotropic numerical model of the survey region with grid resolution ranging between 2 and 12 kilometers. Corrections to the model for the effects density stratification were made from the previous observations of tidal heights and currents. Use of models to remove tides from observations is limited by the grid resolution and accuracy of the models. The second method used the least squares harmonic method developed by Candela et al., discussed previously. Just like Candela's work in the Yellow Sea, the survey track around Vancouver Island covered an area roughly 50 km by 50 km and only the M2 and K1 constituents were resolved. Through inference, additional tidal constituents (e.g., S2 and O1) could be included in the analysis. Through analysis of the ADCP data around Vancouver Island, Foreman and Freeland found that detiding with the barotropic model performed much better than detiding by harmonic analysis. Reasons for the poor performance of the harmonic analysis include having only three days of observations to separate semi-diurnal and diurnal forcing and that M2 and K1 constituents around Vancouver Island are similar in magnitude, unlike in the Yellow Sea where M2 is dominant.

The work of Munchow et al. [20] looked into extracting sub-tidal velocity signals from shipboard ADCP surveys. The methods developed by Simpson et al., Candela et al., and a new method using interpolation of stationary current meter data was used to remove tidal currents. The survey was conducted at the mouth of Delaware Bay and covered three separate transects all roughly 20 km long; one at the mouth of the bay, one north along the coast, one south along the coast. A 300 kHz ADCP was used to conduct the survey. The maximum water depth was 25 m. Based on the observations of ADCP data and bottom track return, a threshold of 2 m/s was identified as the maximum ship speed for obtaining high-quality measurements. Munchow et al. [20] was able to use shipboard ADCP data from repetitive tracks to resolve both tidal and sub-tidal currents, as well as a baroclinic jet.

### 3.2 Methodology

In Admiralty Inlet, the currents during a strong spring tide exceed 3 m/s and because both M2 and K1 constituents have considerable amplitude, the methods developed by Candela et al. [3] and Simpson et al. [26] must be applied with caution. The method developed here for Admiralty Inlet has observational and data collection similarities to previous work, but incorporate a new analysis technique. The technique uses short shipboard surveys of 4 to 5 hours to characterize spatial variation of the entire tidal current process instead of analyzing individual constituents which requires surveys of longer duration. Surveys on ebb or flood tides were conducted during research cruises in August 2009, November 2009, February 2010, and May 2010.

The survey track is a single lap which the ship transits repeatedly during an ebb or flood cycle. Each lap measures the currents at a different stage of the tidal cycle. Survey laps are conducted both before and after the peak ebb or flood peak currents. This timing can be either established by real time analysis during a survey or estimated in advance from a tidal current prediction. Surveys are conducted from the University of Washington Applied Physics Lab Research Vessel Jack Robertson. The ADCP is a hull-mounted, downward looking, Teledyne RDI Workhorse Monitor. The instrument configuration is summarized in Table 10. The ADCP uses bottom tracking to filter out ship motion from measured water velocities. If the bottom reference is lost, ADCP measurements are badly degraded.

**Table 9 – Shipboard ADCP Configuration**

Teledyne RDI Workhorse Monitor	
Acoustic Frequency	307.2 kHz
Time per Ping	0.5 sec
Time between Pings	3 - 4 sec
Vertical Bin Size	1.0 m
Pings / Ensemble	1
Transducer Depth	1.18 m
Blanking Distance	2.0 m

On each lap, the ship passes a given spatial location “A”. Ideally, spatial location “A” is approximately passed on each lap. Due to the strength of currents, wind, and waves the track actually varies between each lap and location “A” is never strictly reoccupied. Individual ADCP pings can, however, be horizontally binned when computing an ensemble.

All ensemble (time and space) averaging is conducted during post processing of the shipboard ADCP, allowing for the user to define ensemble parameters to achieve desirable statistics (e.g., smallest bins with low measurement noise).

A few different factors determine whether or not an individual ping will be successfully received and processed by the ADCP, but the most important is the speed of the ship. Ship speeds in excess of 3.0 m/s when combined with excessive pitch and roll, do not allow sufficient time for the ADCP to receive the bottom track, while ship speeds below 1.5 m/s do not provide desirable spatial coverage or allow effective steering in strong currents. When the surface of the water is calm and the currents are weak, maintaining consistent ship speed is straightforward, but when currents are strong and surface is rough (as is common in Admiralty Inlet) this can be a challenge.

For best results, the duration of the survey must capture both peak currents and more than two hours of the tidal cycle from leading up to and coming off a peak. Specific to this site, some flood cycles exhibit a secondary peak prior to the true peak. Therefore, it is very important to observe enough of the cycle to distinguish primary and secondary peaks.

Survey tracks are designed so longer segments are perpendicular to the dominant current direction and shorter segments run parallel with the currents. Maintaining constant ship speed (the main factor in a good ADCP return) is easier to achieve moving cross-current (crabbing) because the currents do not act along the heading of the ship. The shorter segments of a track may be compromised if currents substantially increase ship speed. An example ebb survey track for Admiralty Inlet is shown in Figure 29. For flood surveys, there is a slight rotation to adjust for variation in the dominant current direction vs. the orientation of the longer track legs. In addition, the February 2010 ebb survey track passed over the May-August and the August-November stationary ADCP deployments. In future work, this may provide a long-term prediction for currents at one point on the track that could be extrapolated to estimate the power generation potential at other points.

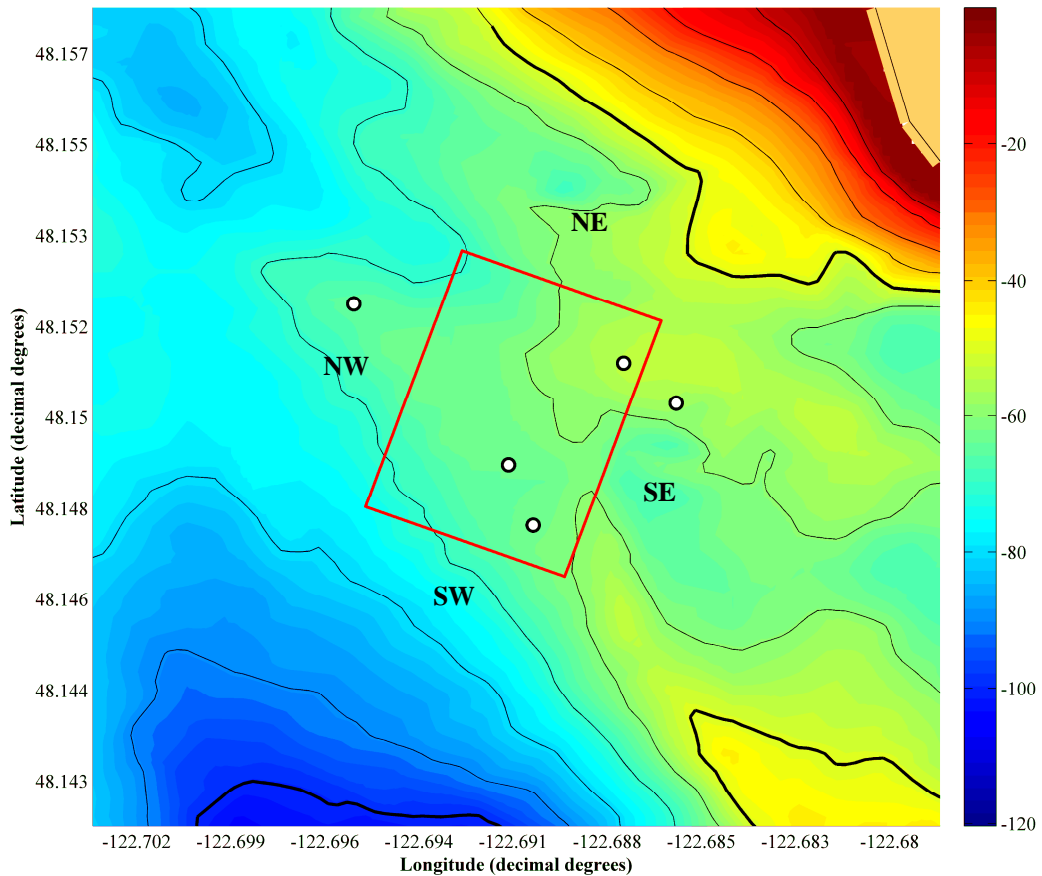


**Figure 29 – Shipboard ADCP ebb survey track in Admiralty Inlet from August 2009. The survey track is superimposed over water depth (m). White circles denote the locations of stationary ADCP deployments.**

To plan a survey, tidal current predictions from stationary ADCP harmonic analysis results provide an estimate of peak currents which survey start time and duration can be based on. If a survey pattern is too long in duration, the timing between each lap may result in large gaps in the time series for a bin and inaccurate identification of peak currents. For the Admiralty Inlet site, lap duration of approximately twenty minutes strikes a balance between adequately resolving the spatial variability in the currents and maximum vessel speed for good ADCP returns. This scheme allows a station to be periodically missed without compromising the time series generated from the ADCP measurements.

Each lap is divided into 100m x 100m bins along nominal ship track which accommodates variability between different laps. Each ADCP measurement (ping) is sorted into one of the spatial bins, or discarded if outside the bin boundaries. For example, during ebb and flood surveys in November 2009, several tracks did not pass through any bins due to rough weather. There are four track segments (NW, NE, SE, and SW), as seen in Figure 29. The alignment and location of the bins is

chosen to maximize the number of pings which fall within at least one track bin. In Figure 30, the variation between different laps of all the surveys can be seen. The November 2009 surveys have large differences between the individual laps which prevented the successful binning of the data for analysis. The two laps from the August 2009 ebb survey which have considerable drift are due to CTD cast operations coincident with velocity surveys.

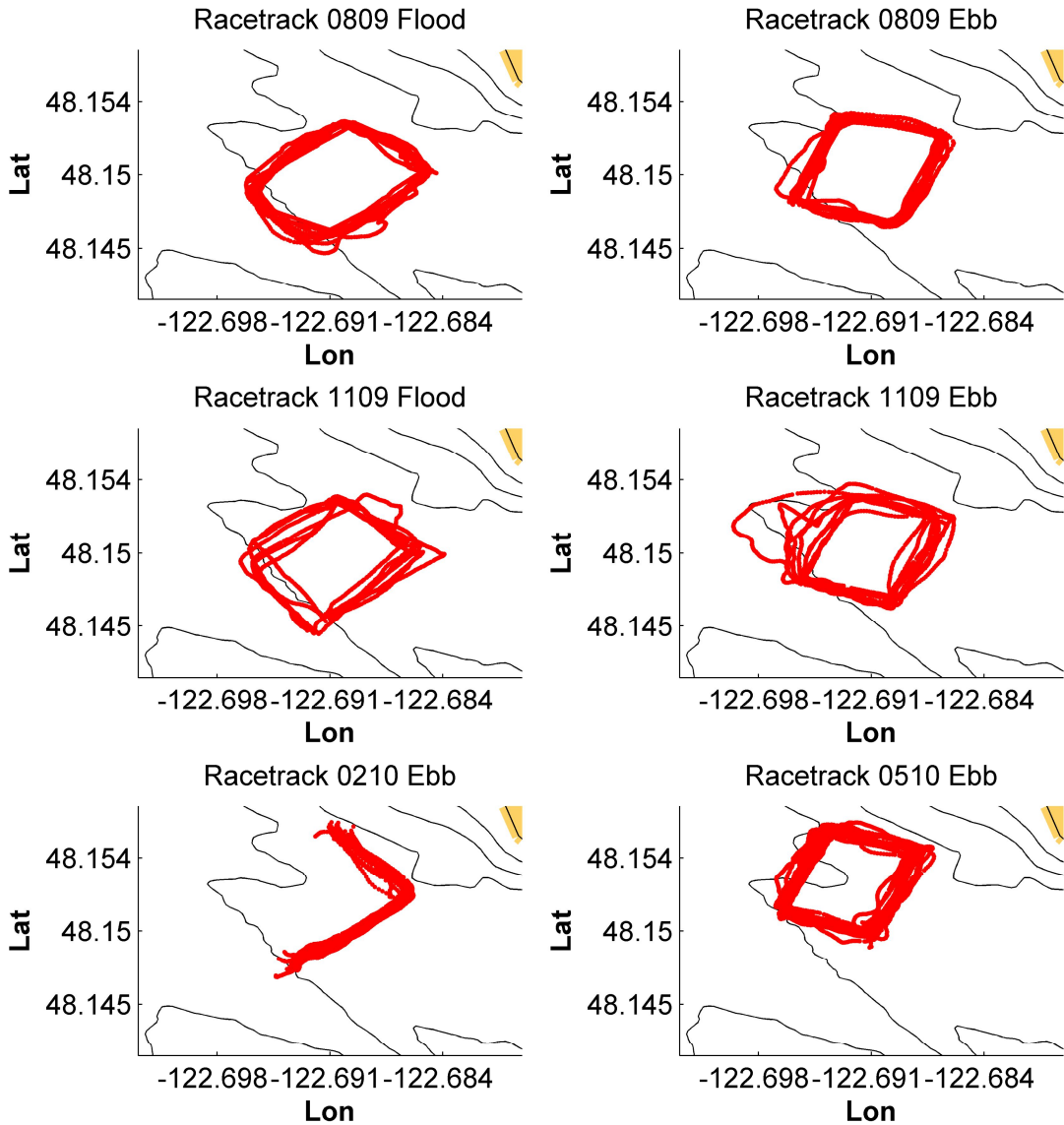


**Figure 30 – Vessel path from all shipboard ADCP ebb and flood surveys. Each red point is an individual ADCP ping.**

Approximately one minute is required to transit each bin at 1.5 m/s vessel speed, which is determined by previous experience to be the practical limit for maintaining good ADCP returns. However, due to the strength of the currents in Admiralty Inlet, as well as wind and waves, there is always a variation in ship speed and course which difficult to plan for prior to the survey. Due to these circumstances, the actual speed at which the laps were transited often exceeded 1.5 m/s. Good ADCP returns are possible from surveys which exceed 1.5 m/s but the sensitivity of the ADCP return to factors such as pitch and roll of the ship increase. Below is a table of the min and max average velocities for all laps during each of the six surveys.

**Table 10 – Shipboard ADCP survey summary from Admiralty Inlet**

Shipboard Survey	Currents	# laps	Average Lap Duration	Vessel Speed
August 3, 2009	Flood	10	22.5 min	1.4 - 2.7 m / s
August 5, 2009	Ebb	12	18.1 min	1.6 - 2.8 m / s
November 11, 2009	Flood	7	25.1 min	1.3 - 4.8 m / s
November 11, 2009	Ebb	9	20.2 min	1.4 - 2.6 m / s
February 10, 2010	Ebb	13	10.8 min	1.7 - 4.0 m / s
May 4, 2010	Ebb	14	18.9 min	1.4 - 3.3 m / s

In order to ensure robust statistics, each 100 m x 100 m bin along the tracks is extended 5 m in the vertical, as shown in Figure 31 and Figure 32. It is assumed that currents are relatively uniform within these ensemble volumes. Close to the seabed, the velocity profile changes considerably with depth and the presumed homogeneity over 5m depth averaging should be viewed with caution. To calculate an accurate mean velocity for each bin, a minimum of thirty pings is found to be necessary to reduce the inherent instrument noise. The typical spread for individual profiles (single ping) versus volumetric ensembles is shown in Figure 32. The track bin labeled “1” in Figure 31 is selected as a representative bin with relatively good ADCP returns and is used as a reference for the remainder of this analysis.

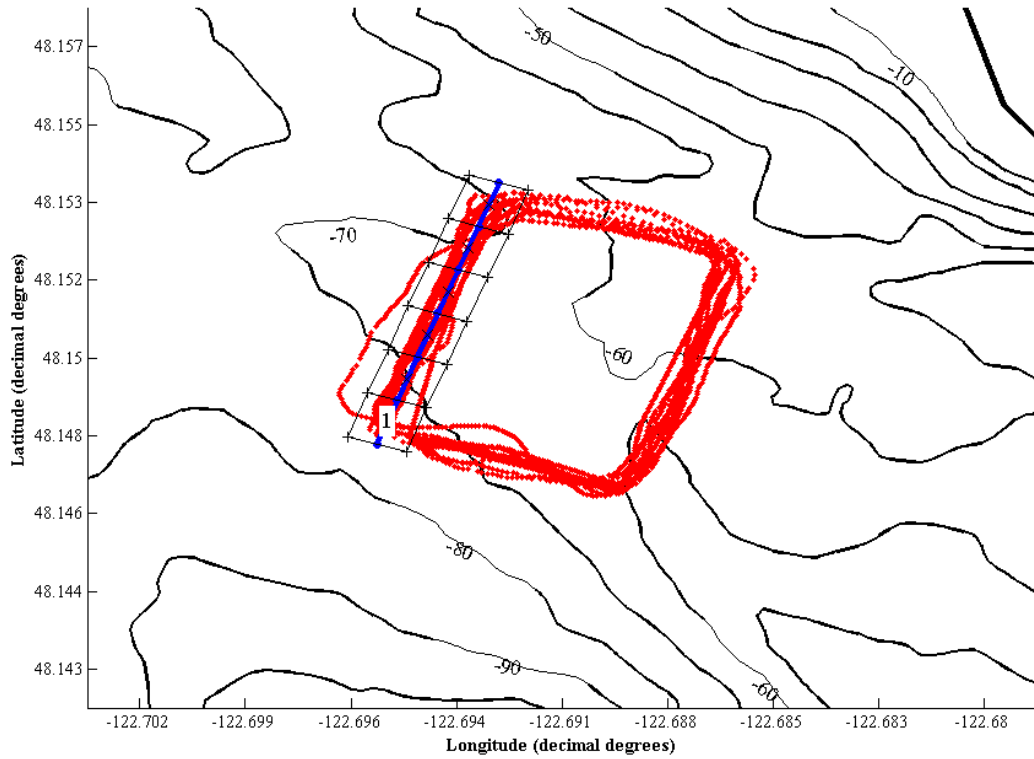


Figure 31 - Individual pings in red with bin centerlines and outlines from August, 2009. The bin labeled 1 is chosen as representative for the following analysis.

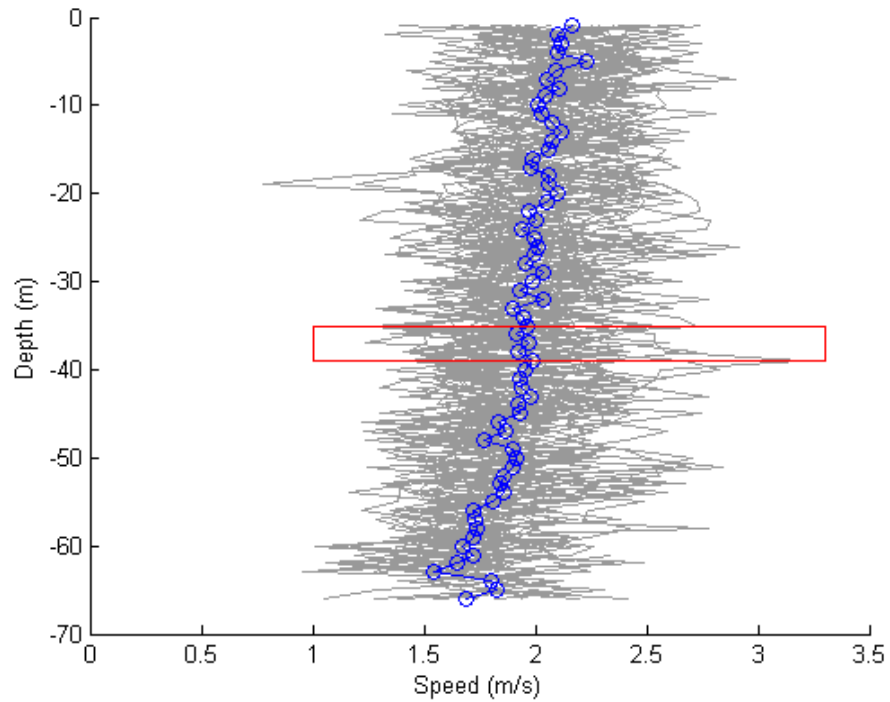
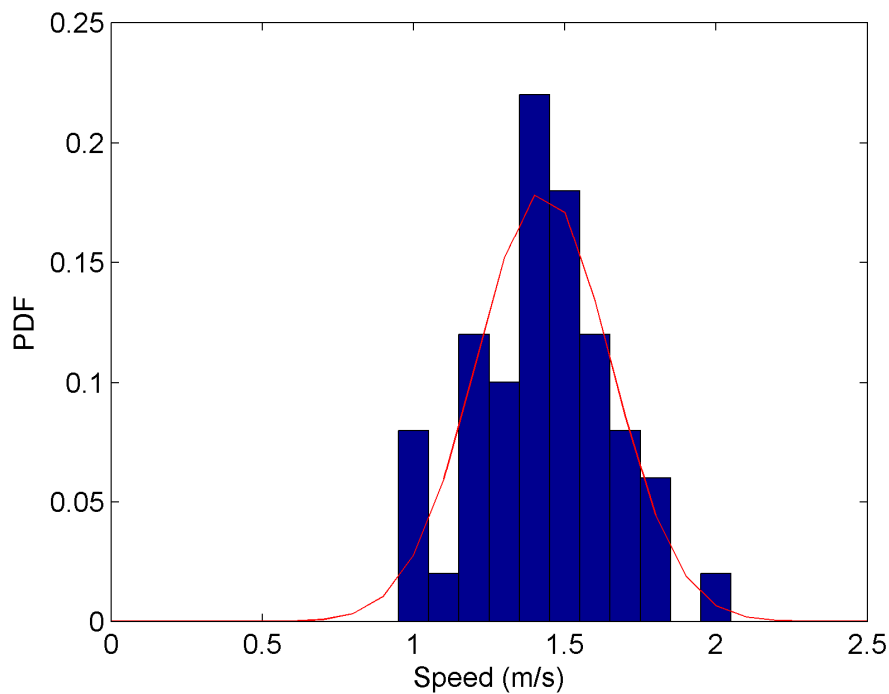


Figure 32 - Individual ADCP ping velocity profiles (gray) for August 2009 ebb survey, horizontal bin averages for 1 m vertical (blue), 5 m vertical average region (red box).

Confidence intervals are required to understand the statistics of the volumetric ensembles. Because the mean and standard deviation of the population are unknown, these must be estimated from the sample mean and standard deviation. With this survey there are sufficient pings/ensemble for normal statistics to be used. However, a *t*-distribution, which converges to a normal distribution for a large sample sizes, is used for conservatism. The following equation is used to generate 99 % confidence intervals for the ensembled velocity where  $\bar{x}$  is the sample mean,  $s$  is the sample standard deviation and  $n$  is the sample size.

$$\bar{x} \pm 2.58 \times \frac{s}{\sqrt{n}}$$

The calculation of confidence intervals do not require that the sample mean be normally distributed and different distributions for the sample mean would affect the sample standard deviation, thus changing confidence interval bounds. Considering the distribution of individual ADCP pings in Figure 32, we see that the individual mid-water column velocities are normally distributed about the sample mean. This confirms that the volumetric ensemble is not likely to be smoothing spatial variations in velocities for this bin size. If the currents were biased over the sample volume, the distribution could be expected to have multiple peaks or a non-normal distribution.



**Figure 33 – Histogram of ADCP Pings (blue) w/ Normal PDF (red) corresponding to sample mean and standard deviation**

The ensemble averages for each lap passing through each bin form a short time series, encompassing the time of peak current. Once the short time series has been developed, the data are fit by a sine wave using the unconstrained nonlinear optimization routines built in to MATLAB. The amplitude ( $A$ ), phase ( $\Phi$ ), and period ( $T$ ) of the sine fit are all free parameters and the optimization essentially converges to a least squares solution. However, this is based on the assumption that each stage of the tide (slack→peak & peak→slack) can be represented as a single sinusoid of a certain period, phase, and amplitude. To improve convergence, the initial estimates for these parameters are taken from NOAA current predictions for the station 0.5 miles west of Admiralty Head. The fit to the velocity curve ( $u$ ) is assumed to be of the form

$$u(t) = A \sin\left(\frac{2\pi t}{T} + \phi\right).$$

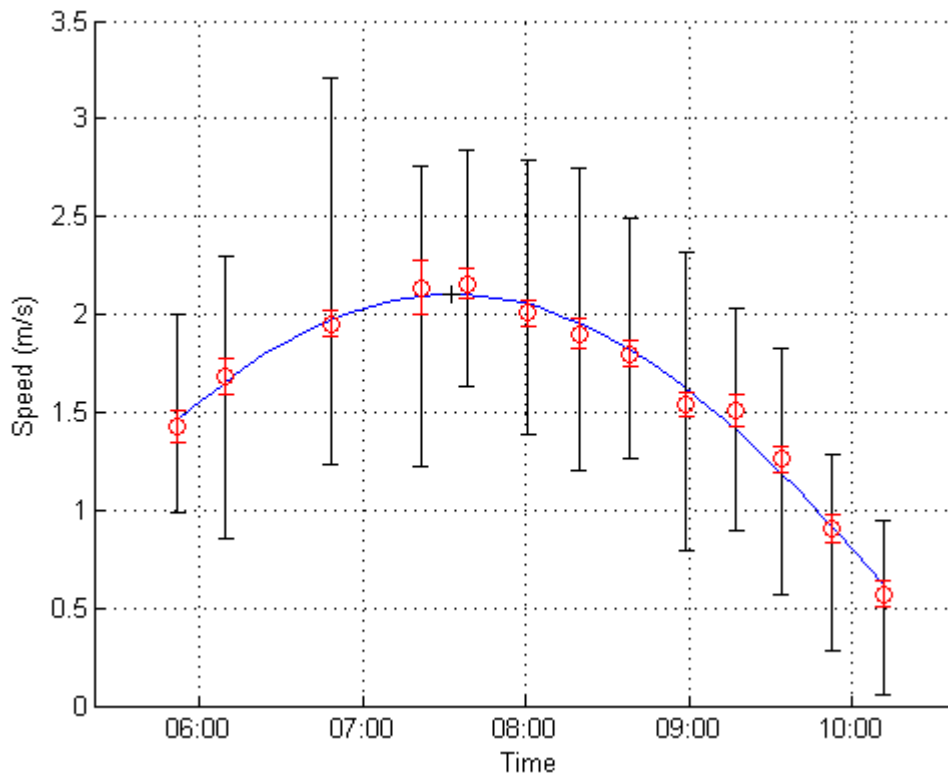


**Figure 34 - Ensemble averaged data (red circles) with half period sine fit (blue) are shown for the ensemble volume noted as 1 on Figure 31, obtained during the August 2009 survey. The red lines denote the 99% confidence interval for the means. The black bars denote the maximum and minimum values within the ensemble. The coefficient of multiple determination for the sine fit is 0.99.**

The half period sine fit in Figure 34 is representative of a high-quality bin. Bin quality is defined by an acceptance criteria consisting of:

1. The ensemble volume contains at least 30 pings;

2. There are at least five volumetric ensemble averages (data points) on the tidal curve;
3. The period determined by the optimization is less than 8.5 hrs;
4. The time of peak amplitude from the sine fit is contained within the series; and
5. The coefficient of multiple determination, R-squared is less than 0.80.

The acceptance criteria is chosen empirically to easily accept bins where the fit is conclusive as well as bins where the fit is less conclusive but follow the trend of the surrounding good bins. Including bins based on trending is an iterative process, whereby the allowable R-squared value is decreased until bins with multiple outliers are rejected, while marginal bins are accepted. If a bin did not meet all the acceptance criteria, then it was excluded from the subsequent analysis. Future analysis could focus on better understanding the factors leading to a poor fit.

The sine fit is only an approximation of the actual tidal currents, which are a superposition of several sinusoidal tidal constituents, turbulence, bathymetric influence, and baroclinic currents. These currents have distinct differences in period leading up to and after peak currents, which is ignored by the half period sine wave fit. Attempts have been made to use a quarter period sine fit to resolve differences in period before and after the peak current, but because no surveys encompass both peak currents and slack water, these are by nature, extrapolations, and subject to unacceptably high uncertainty.

### 3.3 Results & Discussion

The resulting survey data that passes all acceptance criteria are used to compare the peak currents and phase differences over the different ebb and flood survey tracks, as shown in Figure 30. The amplitude variations at these bin resolutions demonstrate that length scales on the order of hundreds of meters need to be characterized. When deploying the OpenHydro tidal turbines for the SnoPUD pilot project, the final siting location should be at the location of peak velocity. During the NNMREC survey cruises in August 2009, November 2009, and February 2010, and May 2010, four ebb and two flood current surveys were completed. Comparisons are made between like surveys (ebb or flood) for current amplitude and peak timing, normalized to allow comparison between ebbs and floods of different magnitudes. The normalization is relative to the easternmost bin, chosen because two of the racetracks pass through that bin. However, this selection is somewhat arbitrary and the normalization reference could be taken at any point along the survey track. As shown in Figure 35, the trends in normalized current amplitude are consistent between the three surveys and independent of current strength or time of year. The November 2009 ebb survey is excluded from the analysis because no bins met all acceptance criteria. Variations in the flood surveys are not as pronounced and a large proportion of track bins are not accepted, resulting in sparse data. One explanation for the dissimilar variation between ebbs and floods could be the influence of eddy formation (in the survey area) off of Admiralty Head during ebb, but not flood.

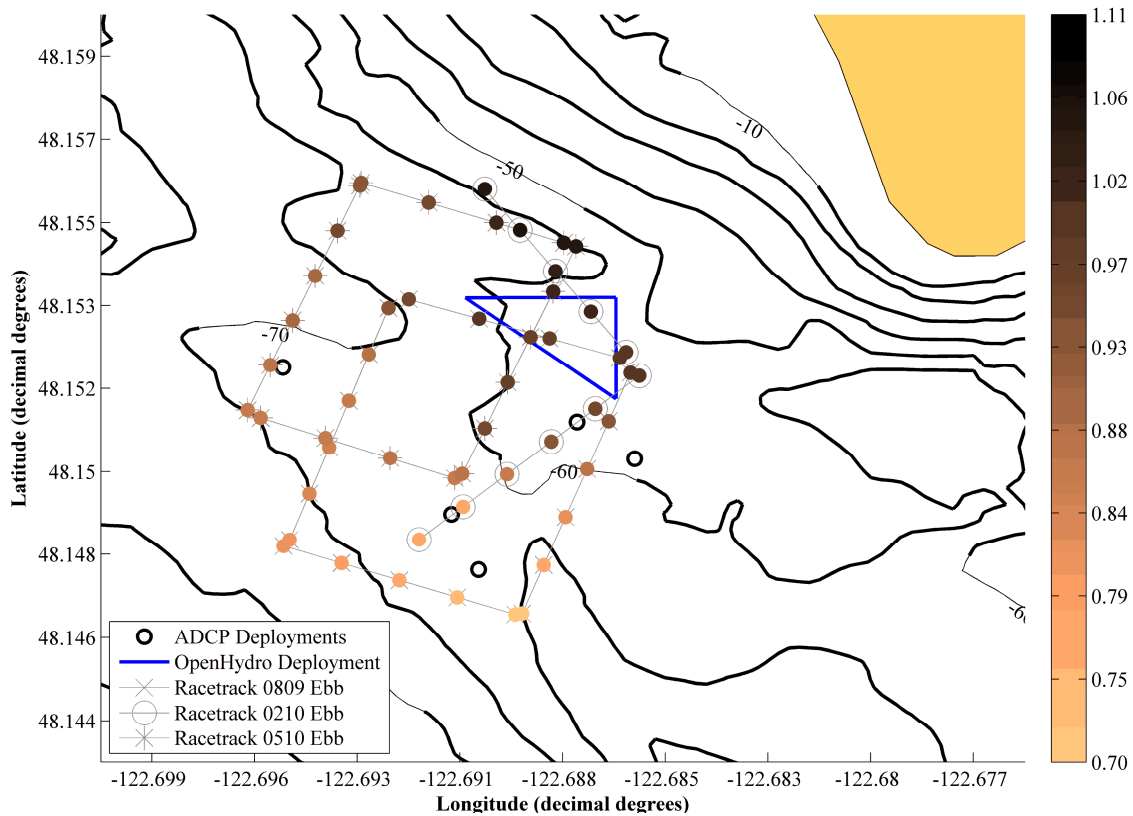


**Figure 35 – Normalized peak ebb current amplitude for the August 2009, February 2010, and May 2010 surveys at mid-water column. The contours are water depth (m).**

The agreement between the three ebb surveys is encouraging since these ebbs were surveyed at different times over a nine month period. Resolving amplitude variation between multiple surveys of only 4-5 hours duration represents a novel method to resolve current strength. Additionally, by overlapping surveys successively, greater coverage can be achieved without increasing track length or vessel speeds. The ebb current amplitudes increase towards the headland, which is in agreement with the site metrics in Table 1 that from stationary ADCP analysis. This suggests that the currents sea spider deployment at the center of the OpenHydro deployment triangle will be more energetic than other locations characterized by stationary ADCP surveys.

A phase map of peak ebb currents is less conclusive.

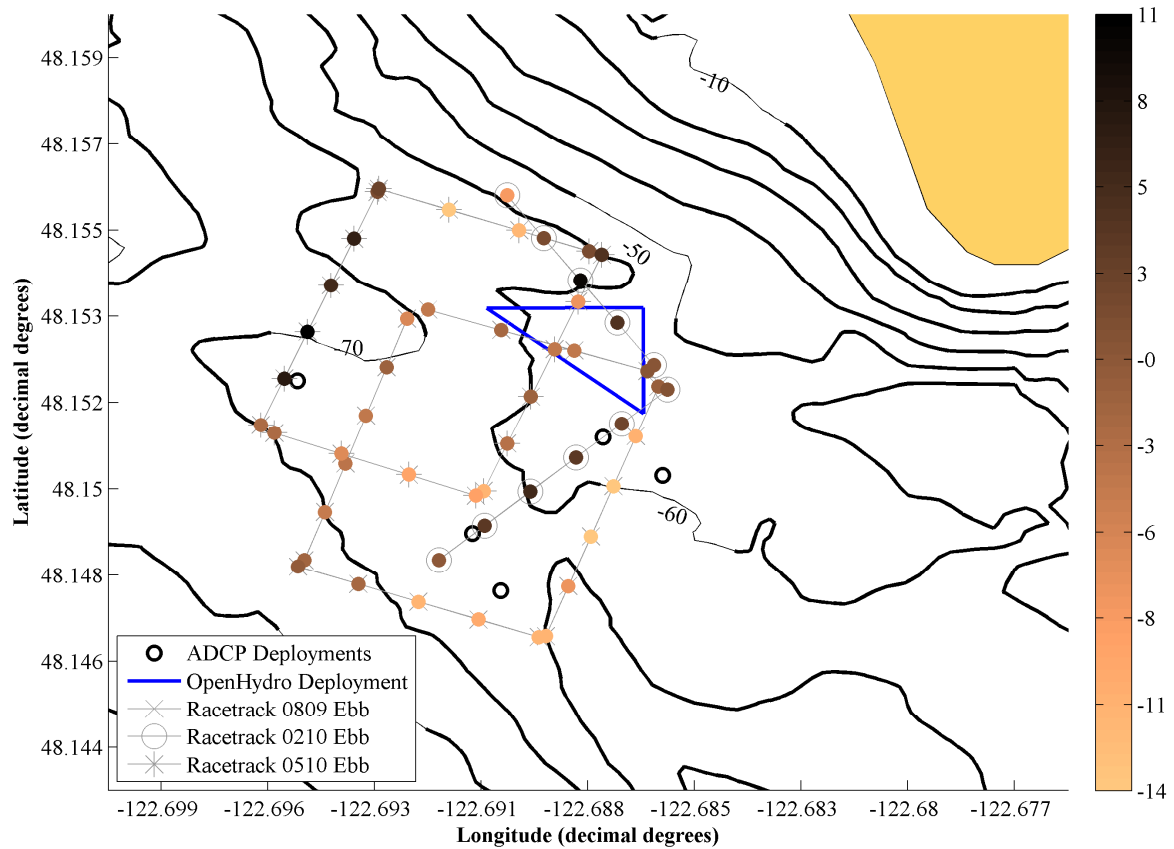


**Figure 36 – Peak ebb current phase (minutes relative to easternmost bin) for the August 2009, February 2010, and May 2010 surveys. Contours are water depth (m).**

Looking at the phase of the peak currents and comparing to the amplitude map, there are no discernable trends between or within surveys. The August 2009 survey suggest a minor trend to the timing of peak currents, with a phase difference of roughly 15 minutes over the track. The tidal curves from the August 2009 ebb survey have at least three points prior to and after the time of peak currents. In contrast, the tidal curves from the May 2010 survey contain only one or two points after the estimated peak ebb. Since the survey tracks require, on average, 18 minutes, the calculated phase differences are generally of the same order as experimental uncertainty and it may be reasonable to conclude that there is not a statistically significant variation in phase for ebb tides.

The amplitude and phase maps from the August and November 2009 flood surveys follow.

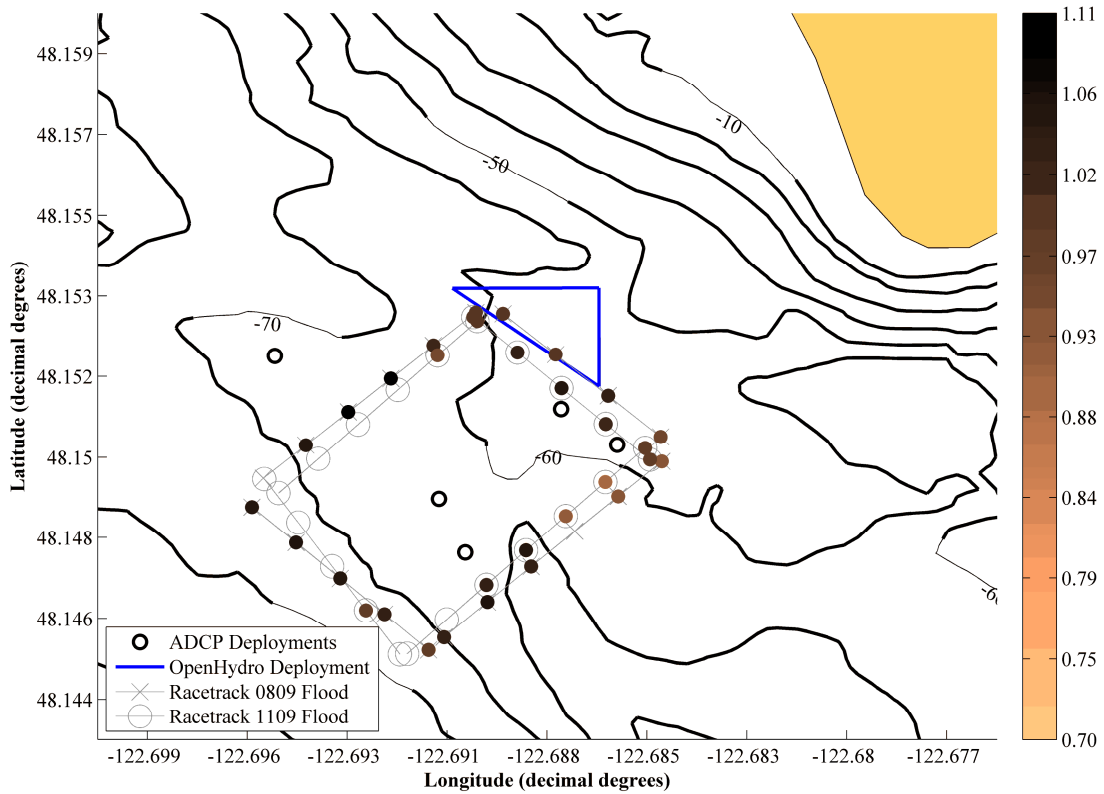


**Figure 37 - Normalized peak flood current amplitude for the August 2009, November 2009 surveys at mid-water column. The contours are water depth (m).**

Amplitude variation over the site is much less distinct during periods of flood currents. Smaller spatial range of peak currents in the flood surveys demonstrates the variability between ebb and flood cycles are not equal. For the November 2009 flood survey, 10 of 23 volumetric bins did not satisfy the acceptance criteria outlined in the previous section. Reasons for bin rejection were mixed between insufficient ensemble size, less than 5 points in the mean velocity time series, and R-squared values below 0.8. The accepted data the trends are certainly different and likely due to the flow around the headland and over the bathymetry. Differences in phase however are more pronounced.

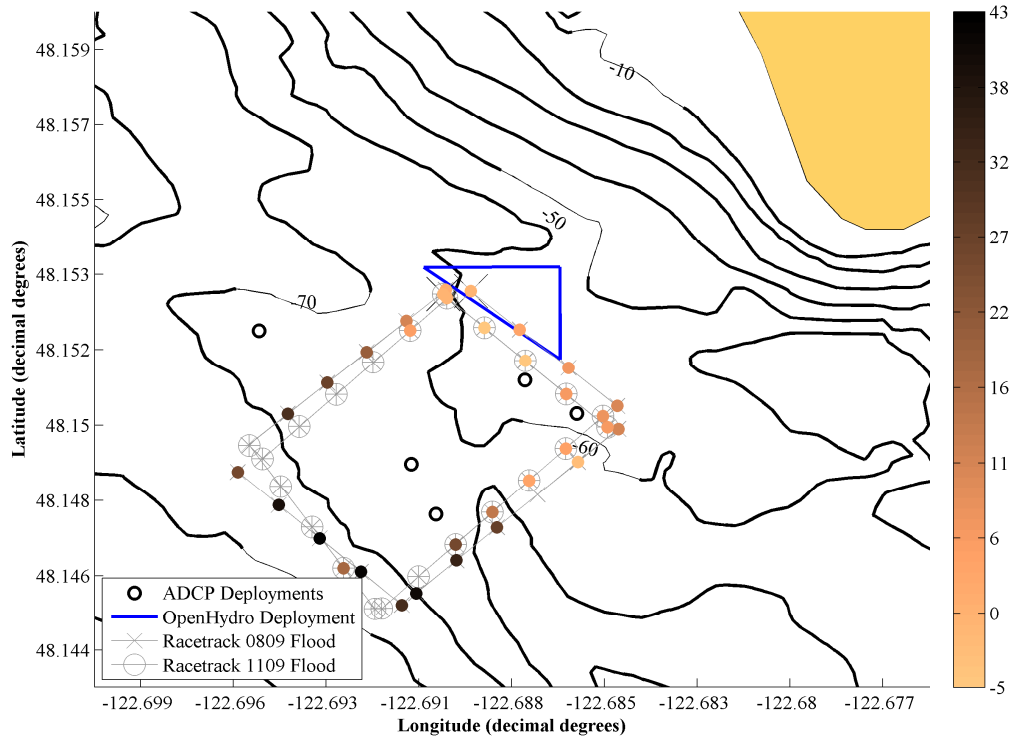


**Figure 38 - Peak flood current phase (minutes relative to northernmost bin) for the August 2009, November 2009 surveys. Contours are water depth (m).**

Phase difference through the site peak at almost 50 minutes as compared to 25 minutes for ebb surveys which cover a larger spatial area.

From these results, the site experiences large current magnitude differences with small phase variation during ebb currents, and small magnitude differences with large phase variations during flood currents. Characterizing this kind of behavior at the site provides additional information about the ebb/flood asymmetry.

Fitting the observed tidal currents with a half period sine wave is not without its limits. Primarily, the half period sine fit does not allow for known asymmetry in the timing from slack to peak and peak back to slack. A quarter period sine fit to the data before and after peak could provide this flexibility. All the surveys conducted to date do not survey through slack water and, therefore, the timing of slack water must be extrapolated. Initial attempts to fit quarter period sine waves show promise in some cases. Below is a quarter period sine fit to the same averaged data shown in Figure 34. During the first lap of the survey the ebb current is nearly 1.5 m/s and extrapolation to slack water would be

questionable. However, the survey does extend for almost 2.5 hours after the peak current and estimating the timing of slack water and, therefore, quarter period could be reasonable.

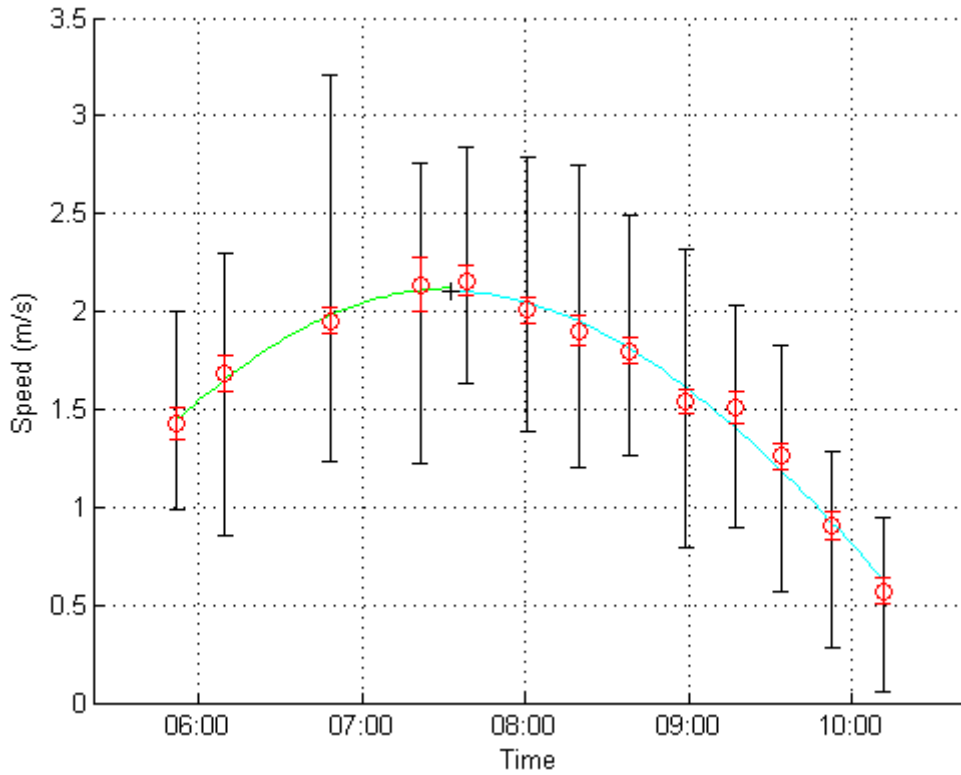


**Figure 39 - Ensemble averaged data (red circles) with quarter sine fits (light blue and green lines) are shown for the ensemble volume noted as 1 on Figure 31, obtained during the August, 2009 survey. The red lines denote the 99% confidence interval for the means. The black bars denote the maximum and minimum values within the ensemble. The coefficient of multiple determination is 0.99.**

The use of short duration shipboard ADCP surveys to characterize a site informs decisions on where to deploy additional stationary ADCPs or hydrokinetic devices. New surveys that are conducted from slack water through the time of peak currents might be better suited to being reliably fit by a quarter period sine wave.

## 4 Conclusion

The current observations from Admiralty Inlet site provide a unique tool to test methods for characterization of tidal resources. Admiralty Inlet has very strong currents, providing a rugged test case for the stationary and shipboard methods before applying them to other sites. The efforts serve as a first step towards establishing universally applicable methods.

Currents at this site are neither bi-directional nor elliptical. Different treatments of these data prior to harmonic analysis result in comparable accuracy, but residual analysis demonstrates unresolved variability at all frequencies which may require different techniques (e.g., empirical orthogonal functions) to characterize.

Further work could consider the assimilation of stationary and shipboard ADCP surveys. The long time series captured by stationary ADCPs are suited for harmonic analysis and, therefore, predictions of tidal currents. The spatial variability of in current amplitude captured by limited shipboard ADCP surveys shows this to be an efficient tool for mapping currents. A first concept for assimilation would deploy a stationary ADCP in an area for a three month period to characterize the currents at one location. To resolve nearby spatial variability, a shipboard survey could map how amplitudes vary relative the stationary location. Assuming the survey passes over the stationary deployment, the amplitude ratios can normalized to the stationary location and provide a means to scale current predictions from the harmonic analysis throughout the area and provide a coarse prediction for each bin along the survey track. This could prove an invaluable tool for power generation estimates.

## REFERENCES

- 1 Boon, John D. (2004), *Secrets of the Tide: Tide and Tidal Current Analysis and Predictions, Storm Surges and Sea Level Trends*, Horwood Publishing Limited, Coll House, England.
- 2 Brown, J., E.D. Barton, A. Trasvina, H.S. Velez, P.M. Kosro, and R.L. Smith (1992), Estimation of Surface Winds From Upward Looking Acoustic Doppler Current Profilers, *Journal of Geophysical Research*, 97(C11), 17925-17930.
- 3 Candela, Julio, Robert C. Beardsley, and Richard Limeburner (1990), Removing Tides from Ship-Mounted ADCP Data, with Application to the Yellow Sea, in *Proceedings of the IEEE Third Working Conference on Current Measurement*, 258-266.
- 4 Doodson, A. T., (1921), The Harmonic Development of the Tide Generating Potential, *Proceeding of the Royal Society*, 100, 305-329.
- 5 Devore, J. and N. Farnum (2005), *Applied Statistics for Engineers and Scientists*, Thomson Brooks/Cole, Belmont, CA, USA.
- 6 Emery, W. J., R. E. Thomson (2001), *Data Analysis Methods in Physical Oceanography*, Elsevier, Amsterdam, Netherlands.
- 7 Finlayson D.P., (2005), Combined bathymetry and topography of the Puget Lowland, Washington State, University of Washington, < <http://www.ocean.washington.edu/data/pugetsound/>>.
- 8 Foreman, M. G. G. (1977), Manual For Tidal Heights Analysis and Prediction, *Pacific Marine Science Report*, 77(10).
- 9 Foreman, M. G. G. (1978), Manual For Tidal Currents Analysis and Prediction, *Pacific Marine Science Report*, 78(6).
- 10 Foreman, M. G. G. and H. J. Freeland (1991), A Comparison of Techniques for Tide Removal From Ship-Mounted Acoustic Doppler Measurements Along the Southwest Coast of Vancouver Island, *Journal of Geophysical Research*, 96(C9), 17007-17021.
- 11 Foreman, M. G. G., William R. Crawford, and Richard F. Marsden (1995), De-tiding: Theory and Practice, *Coastal and Estuarine Studies*, 47, 203-239.
- 12 Fraenkel, P. L. (2006), Tidal Current Energy Technologies, *International Journal of Avian Science*, 148(1), pp. 145-154.

- 13 Geyer, W. Rockwell and Richard Signell (1990), Measurements of Tidal Flow Around a Headland With a Shipboard Acoustic Doppler Current Profiler, *Journal of Geophysical Research*, 95(C3), 3189-3197.
- 14 Godin, Gabriel (1972), *The Analysis of Tides*, University of Toronto Press, Toronto, Ontario, Canada.
- 15 Godin, Gabriel, The Analysis of Tides and Currents (Review), in *Tidal Hydrodynamics*, edited by B. B. Parker, pp. 675-709.
- 16 Gooch, S. (2009), Siting Methodologies for Tidal In-Stream Energy Conversion (TISEC) Systems, M.S. thesis, 79 pp., University of Washington, Seattle, Washington, USA.
- 17 Gordon, R. L. (1996), *Acoustic Doppler Current Profiler: Principles of Operation A Practical Primer*, RD Instruments, San Diego.
- 18 Leffler, Keith E., David A. Jay (2008), Enhancing tidal harmonic analysis: Robust (hybrid L1/L2) solutions, *Continental Shelf Research*, doi: 10.1016/j.csr.2008.04.11.
- 19 Lavelle, J. W., H. O. Mofjeld, E. Lempriere-Doggett, G. A. Cannon, D. J. Pashinski, E. D. Cokelet, L. Lytle (1988), *A Multiply-Connected Channel Model of Tides and Tidal Currents in Puget Sound, Washington and A comparison with Updated Observations*, NOAA Technical Memorandum ERL PMEL-84.
- 20 Munchow, Andreas, Richard W. Garvine, and Timothy F. Pfeiffer (1992), Subtidal currents from a shipboard acoustic Doppler current profiler in tidally dominated waters, *Continental Shelf Research*, 12(4), 499-515.
- 21 Munk, W. J., and D. E. Cartwright (1966), *Tidal Spectroscopy and Prediction*, Series A. Mathematical and Physical Sciences, No. 1115, Vol. 259, pp. 533-581, Royal Society Burlington House, London.
- 22 Northwest National Marine Renewable Energy Center, (2010) <<http://depts.washington.edu/nnmrec>>.
- 23 Pawlowicz, Rich, Bob Beardsley, and Steve Lentz (2002), Classical tidal harmonic analysis including error estimates in MATLAB using T\_TIDE, *Computers and Geosciences*, 28, 929-937.
- 24 Polayge, Brian, Andrea Copping, Keith Kirkendall, George Boehlert, Sue Walker, Michele Wainstein, and Brie Van Cleve (2010), Environmental Effects of Tidal Energy Development: A Scientific Workshop.
- 25 Proctor, R. and J. Wolfe (1983), An Investigation of the storm surge of 1<sup>st</sup> February 1983 using numerical models, in *Focus on modeling marine systems*, edited by A. M. Davies.

26 Simpson, J. H., E. G. Mitchelson-Jacob, and A. E. Hill (1990), Flow structure in a channel from and acoustic Doppler current profiler, *Continental Shelf Research*, 10(6), 589-603.

# Appendix 1- Rayleigh Criterion Constituent Inclusion Charts

**Table 2** Order of Constituent Selection in Accordance with the Rayleigh Criterion. Tidal Potential Amplitude for Main Constituents is Shown within Brackets. Lines with Arrows Denote Links with Rayleigh Comparison Pairs.

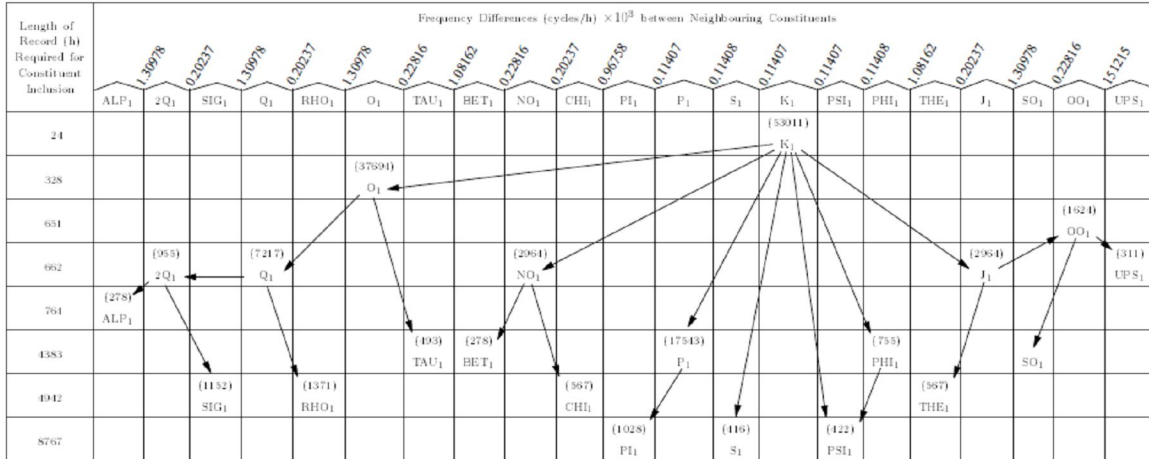
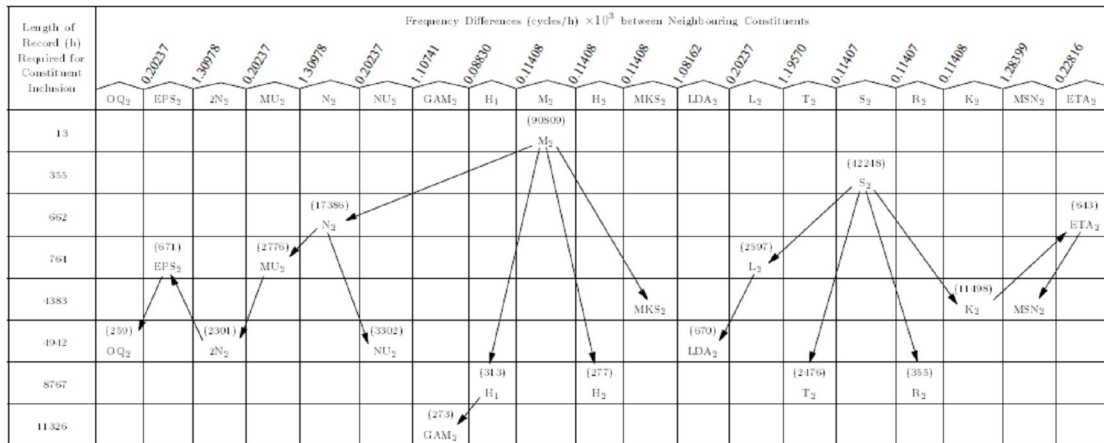


**Table 3** Order of Semidiurnal Constituent Selection in Accordance with the Rayleigh Criterion. Tidal Potential Amplitude for Main Constituents is Shown within Brackets. Lines with Arrows Denote Links with Rayleigh Comparison Pairs.



12

## Appendix 2 - Shallow Water Constituent Inclusion Criteria

**Table 5** Shallow Water Constituents in the Standard Data Package.

Shallow Water Constituent	Record Length (h) Required for Constituent Inclusion	Component Main Constituents and Record Lengths (h) Required for Their Inclusion in the Analysis					
		S <sub>2</sub>	M <sub>2</sub>	O <sub>1</sub>	K <sub>2</sub>	N <sub>2</sub>	K <sub>1</sub>
SO <sub>1</sub>	4383	S <sub>2</sub>	355	O <sub>1</sub>	328		
MKS <sub>2</sub>	4383	M <sub>2</sub>	13	K <sub>2</sub>	4383	S <sub>2</sub>	356
MSN <sub>2</sub>	4383	M <sub>2</sub>	13	S <sub>2</sub>	355	N <sub>2</sub>	662
MO <sub>3</sub>	656	M <sub>2</sub>	13	O <sub>1</sub>	328		
SO <sub>3</sub>	4383	S <sub>2</sub>	355	O <sub>1</sub>	328		
MK <sub>3</sub>	656	M <sub>2</sub>	13	K <sub>1</sub>	24		
SK <sub>3</sub>	355	S <sub>2</sub>	355	K <sub>1</sub>	24		
MN <sub>4</sub>	662	M <sub>2</sub>	13	N <sub>2</sub>	662		
M <sub>4</sub>	25	M <sub>2</sub>	13				
SN <sub>4</sub>	764	S <sub>2</sub>	355	N <sub>2</sub>	662		
MS <sub>4</sub>	355	M <sub>2</sub>	13	S <sub>2</sub>	355		
MK <sub>4</sub>	4383	M <sub>2</sub>	13	K <sub>2</sub>	4383		
S <sub>4</sub>	355	S <sub>2</sub>	355				
SK <sub>4</sub>	4383	S <sub>2</sub>	355	K <sub>2</sub>	4383		
2MK <sub>5</sub>	24	M <sub>2</sub>	13	K <sub>1</sub>	24		
2SK <sub>5</sub>	178	S <sub>2</sub>	355	K <sub>1</sub>	24		
2MN <sub>6</sub>	662	M <sub>2</sub>	13	N <sub>2</sub>	662		
M <sub>6</sub>	26	M <sub>2</sub>	13				
2MS <sub>6</sub>	355	M <sub>2</sub>	13	S <sub>2</sub>	355		
2MK <sub>6</sub>	4383	M <sub>2</sub>	13	K <sub>2</sub>	4383		
2SM <sub>6</sub>	355	S <sub>2</sub>	355	M <sub>2</sub>	13		
MSK <sub>6</sub>	4383	M <sub>2</sub>	13	S <sub>2</sub>	355	K <sub>2</sub>	4383
3MK <sub>7</sub>	24	M <sub>2</sub>	13	K <sub>1</sub>	24		
M <sub>8</sub>	26	M <sub>2</sub>	13				